https://doi.org/10.5194/acp-2022-247
Preprint. Discussion started: 12 April 2022

Atmospheric Chemistry and Physics Discussions

Ozone depletion in the Arctic and Antarctic stratosphere induced by wildfire smoke

Albert Ansmann[1], Kevin Ohneiser[1], Alexandra Chudnovsky[2], Daniel A. Knopf[3], Edwin W. Eloranta[4], Diego Villanueva[5], Patric Seifert[1], Martin Radenz[1], Boris Barja[6], Félix Zamorano[6], Cristofer Jimenez[1], Ronny Engelmann[1], Holger Baars[1], Hannes Griesche[1], Julian Hofer[1], Dietrich Althausen[1], and Ulla Wandinger[1]

[1]Leibniz Institute for Tropospheric Research, Leipzig, Germany
[2]Tel Aviv University, Porter School of Earth Sciences and Environment, Tel Aviv, Israel
[3]School of Marine and Atmospheric Sciences, Stony Brook University, Stony Brook, NY 11794-5000, USA
[4]Space Science and Engineering Center, University of Wisconsin, Madison, Wisconsin, USA
[5]Leipzig Institute for Meteorology, University of Leipzig, Leipzig, Germany
[6]Atmospheric Research Laboratory, University of Magallanes, Punta Arenas, Chile

Correspondence: A. Ansmann
(albert@tropos.de)

Abstract. A record-breaking stratospheric ozone loss was observed over the Arctic and Antarctica in 2020. Strong ozone depletion occurred over Antarctica in 2021 as well. The ozone holes developed in smoke-polluted air. In this article, the impact of Siberian and Australian wildfire smoke (dominated by organic aerosol) on the extraordinarily strong ozone reduction is discussed. The study is based on aerosol lidar observations in the North Pole region (October 2019 - May 2020) and over Punta Arenas in southern Chile at 53.2°S (January 2020 - November 2021) as well as on respective NDACC (Network for the Detection of Atmospheric Composition Change) ozone profile observations in the Arctic (Ny-Ålesund) and Antarctica (Neumayer and South Pole stations) in 2020 and 2021. We present a conceptual approach how the smoke may have influenced the formation of polar stratospheric clouds (PSCs) which are of key importance in the ozone-depleting processes. The main results are as follows: (a) The direct impact of wildfires smoke (below the PSC height range, at 9-12 km height) on additional ozone reduction seems to be similar to the impact of the well-known volcanic sulfate aerosol effects. Smoke particle surface area (SA) concentration of 5-7 μm^2 cm^{-3} (Antarctica, spring 2021) and 6-10 μm^2 cm^{-3} (Arctic, spring 2020) was correlated with a smoke-related additional ozone loss in terms of ozone partial pressure of 0.4-1.2 mPa (30-50% of the total ozone loss, Antarctica) and 2-3.5 mPa (again 30-50%, Arctic) at heights from 9-12 km. (b) Within PSCs (14-23 km height range), we found indications that smoke was able to slightly increase the PSC particle number and surface area concentration. In particular, a smoke-related additional ozone loss of 1-1.5 mPa (10-20% contribution to the total ozone loss) was observed in the central 15-20 km PSC height range over Antarctica in September-October 2020 and 2021, however, independent of the strength of the smoke pollution, i.e., for smoke particle number concentrations ranging from 10 to 100 cm^{-3} (a factor of 3-10 above the stratospheric aerosol background level). A similar amount of 1-1.5 mPa smoke-related ozone loss was estimated for the PSC height range over the Arctic in spring 2020. Satellite observations indicated an additional mean column ozone loss (deviation

https://doi.org/10.5194/acp-2022-247
Preprint. Discussion started: 12 April 2022

Atmospheric Chemistry and Physics Discussions

from the long-term mean) of 26-30 Dobson units (9-10%, September 2020, 2021) and 52-57 Dobson units (17-20%, October 2020, 2021) in the smoke-polluted latitudinal Antarctic belt from 70°-80°S.

1 Introduction

Since the summer of 2017, three record-breaking wildfire events occurred, specifically, the Canadian wildfire storm on 12-13 August 2017, the strong, long-lasting Siberian fires in July and August 2019, and the Black Summer fire season of 2019–2020 in southeastern Australia. These events caused major perturbations of the stratospheric aerosol conditions in the Northern Hemisphere (NH) (Khaykin et al., 2018; Peterson et al., 2018; Yu et al., 2019; Hu et al., 2019; Ohneiser et al., 2021) as well as in the Southern Hemisphere (SH) (Ohneiser et al., 2020, 2022; Khaykin et al., 2020; Kablick et al., 2020). The Canadian wildfire storm led to the largest smoke contamination of the lower stratosphere over Central Europe and the European continent for more than six months in 2017-2018 (Ansmann et al., 2018; Baars et al., 2019; Das et al., 2021). Siberian fires caused an unexpected, dense Arctic smoke layer which was observable over the North Pole region for almost one year (Ohneiser et al., 2021). The Black Summer fire season was finally responsible for the highest smoke-related stratospheric pollution levels ever measured around the globe (Peterson et al., 2021). The January 2020 mean aerosol optical thickness (AOT) for the latitudinal belt from 20°S to 70°S even exceeded its maximum monthly mean AOT observed after the eruption of Mount Pinatubo (Hirsch and Koren, 2021) and significantly influenced the radiation budget in the SH (Hirsch and Koren, 2021; Yu et al., 2021; Stocker et al., 2021; Fasullo et al., 2021; Heinold et al., 2021).

Record-breaking ozone depletion was detected over the Arctic (DeLand et al., 2020; Inness et al., 2020; Wohltmann et al., 2020, 2021; Manney et al., 2020) as well as over Antarctica (Stone et al., 2021; Rieger et al., 2021) in the smoke-polluted stratosphere during the spring seasons of 2020 (March-April in the NH and September-October in the SH). First evidence for an impact of smoke on ozone depletion was found over the High Arctic during the MOSAiC (Multidisciplinary Drifting Observatory for the Study of Arctic Climate) expedition 2019-2020 (Ohneiser et al., 2021; Voosen, 2021). Lidar observations of smoke layering and ozone profiling with sondes were performed aboard the icebreaker Polarstern in the North Pole region during the auntumn, winter and spring seasons of 2019-2020 (see Fig. 1 regarding lidar and ozonesonde stations used in this study). A much clearer and unambiguous indication for an influence of smoke on ozone reduction was then obtained in the SH in September-December 2020 by comparing our lidar observations of Australian smoke profiles at Punta Arenas (53.2°S), Chile, at the southernmost tip of South America, with respective stratospheric ozone observations at the NDACC (Network for the Detection of Atmospheric Composition Change) ozonesonde stations at Lauder (45°S), New Zealand, and the two Antarctic Neumayer (70.6°S) and South Pole stations (Ohneiser et al., 2022). Also Yu et al. (2021), Stone et al. (2021), and Rieger et al. (2021) concluded that the extraordinarily strong ozone loss over the SH polar region in 2020 was probably partly related to the occurrence of Australian smoke in the stratosphere.

It is well known that strong ozone depletion is linked to the development of a cold and long-lasting Polar vortex and associated extensive formation of polar stratospheric clouds (PSCs) (Tritscher et al., 2021). PSCs play a key role in the chain of processes leading to the activation of chlorine and bromine components that destroy ozone at sunlight conditions. Most of

https://doi.org/10.5194/acp-2022-247
Preprint. Discussion started: 12 April 2022


Atmospheric Chemistry and Physics Discussions

the conversion of halogen reservoir species into reactive forms takes place on the surface of liquid PSC particles. The impact of background and volcanic sulfate aerosol on PSC, halogen activation, and ozone depletion processes is extensively studied and well known and implemented in climate and ozone forecast models (e.g., Solomon, 1999; Solomon et al., 2015; Zhu et al., 2018). In contrast, the role of wildfire smoke particles in these ozone-depleting processes is unknown and not considered in these models. Our knowledge about the chemical, microphysical, and morphological properties of the aged organic, probably glassy aerosol particles after long range transport around the globe for months or even years is rather poor. Hence, it is unknown how efficient these particles can serve as sites for heterogeneous chemical reactions to produce active halogen components and further chemical processes that lead to a prolongation of the lifetime of the active halogen components (Solomon et al., 2022). It is also unknown how efficiently the smoke particles can act as nuclei in PSC formation processes.

In order to integrate smoke-related ozone-depleting processes in existing chemistry climate modeling environments, all aspects of this new atmospheric phenomenon need to be explored in detail in upcoming research projects including laboratory studies, airborne in-situ observations, and modeling efforts. The relevance for the required effort is given by the expectation that the number of major fire storms will increase in the twenty-first century due to progressing climate change (Liu et al., 2009, 2014; Abatzoglou et al., 2019; Dowdy et al., 2019). Hence, we need to consider the smoke-ozone-relationship accurately in models and in the climate change debate. Furthermore, to evaluate the achievements of the Montreal Protocol (Wilka et al., 2021; Feng et al., 2021; Stone et al., 2021), all ozone-loss-relevant influences need to be carefully considered in the analysis on long-term ozone time series. The 1987 Montreal Protocol, and its subsequent amendments during the 1990s, mandated the decrease and eventual cessation of the worldwide production of ozone-depleting substances (ODSs) such as chlorofluorocarbons (CFCs) (Wilka et al., 2021). Within the past few years, ever stronger evidence for global ozone stabilization and a nascent Antarctic ozone recovery has emerged (e.g., Solomon et al., 2017; Weber et al., 2022). Therefore, it is important to identify any deviation from the signatures indicating the long-term healing of the ozone layer and to consider all impacts on ozone depletion in respective modeling studies (Solomon et al., 2022; Bernath et al., 2022).

In this article, for the first time, we systematically investigate the impact of smoke on ozone depletion in the polar stratosphere. We continue and extend the discussion we began in our previous and foregoing publications on the link between aerosol vertical layering and altitude-dependent ozone losses up to 20-25 km height (Ohneiser et al., 2021, 2022). The smoke-ozone data analysis is based on the aerosol measurements with two multiwavelength lidars aboard the icebreaker Polarstern and at Punta Arenas and regular ozone profile observations at Ny-Ålesund (78.9°N) in the Arctic and the Neumayer and the South Pole station on the Antarctic continent (see Fig. 1). For an appropriate smoke characterization, we recently developed a wildfire smoke conversion method to derive number and surface area concentrations from the measured stratospheric smoke particle backscatter and extinction profiles (Ansmann et al., 2021).

The paper is organized as follows. In Sect. 2, we compare the impact of different stratospheric aerosol scenarios (background aerosol, volcanic disturbed aerosol conditions, wildfire-smoke-polluted stratosphere) on PSC formation which is of key importance in the ozone-depleting processes. We introduce a conceptual approach how the smoke may influence PSC formation and thus PSC properties. After a brief description of the instruments (lidar, ozonesondes) and data analysis methods in Sect. 3, we

https://doi.org/10.5194/acp-2022-247
Preprint. Discussion started: 12 April 2022


Atmospheric Chemistry and Physics Discussions

continue with the presentation of the main findings regarding the Arctic 2020 and Antarctic 2020 and 2021 ozone depletion seasons in Sect. 4. The summary and conclusion section 5 outlines the main findings and provides an outlook of next steps.

2 The impact of different stratospheric aerosol scenarios on PSC formation

Goal of this section is to provide a short overview of different stratospheric aerosol scenarios regarding their impact on PSC formation. The presented information is required to be able to follow the discussion of findings and observations presented in Sect. 4. In the focus is the hypothetical approach how smoke particles may get involved in PSC formation and ozone depleting processes. As shown in the sketch in Fig. 2, we can distinguish three main stratospheric aerosol scenarios: clean background conditions, volcanic events with enhanced sulfate aerosol levels, and situations with high concentrations of wildfire smoke particles (dominated by organic particles). The properties of the aerosol and of the PSCs developing in these aerosols are discussed in the following Sects. 2.1, 2.2, and 2.3.

2.1 Clean stratosphere

Tritscher et al. (2021) provides an overview of the aerosol conditions and PSC formation processes in the lower stratosphere at aerosol background conditions. In an undisturbed, clean stratospheric environment, supercooled binary solution (SBS) droplets consisting of water and sulfuric acid predominantly nucleate homogeneously and form the stratospheric background aerosol. Observations show that more than 50% of these sulfate particles within the polar vortex region contain insoluble meteoritic substances (Curtius et al., 2005; Weigel et al., 2014). The particle number concentration is of the order of 5-10 cm^{-3}, the median radius of the lognormal size distribution (accumulation mode) close to 100 nm, and the corresponding effective radius about 150 nm (Deshler et al., 2003; English et al., 2011; Zhu et al., 2018). Under volcanic quiescent and smoke-free conditions, these stratospheric particles cause a 532 nm AOT of around 0.005 (Sakai et al., 2016). The respective mean 532 nm particle extinction coefficient is around 0.1-0.3 Mm^{-1} in the height range from 15-25 km (Sakai et al., 2016; Baars et al., 2019; Ohneiser et al., 2022).

Strong ozone depletion in polar regions requires the development of a cold, stable, and long-lasting polar vortex with temperatures below 195 K and the formation of extended PSC fields. Upon cooling, the SBS droplets start to grow by uptake of additional H_2O as a consequence of the decreasing water vapor pressure of the H_2O-H_2SO_4 solutions. A rapid change in particle composition takes place at around $T_{\mathrm{ice}} + 4$ K, when the droplets have become sufficiently dilute so that small amounts of nitric acid (HNO_3) can condense into the acidic liquid (Koop and Carslaw, 1996; Koop et al., 1997). T_{ice} is the frost point temperature (usually <190 K). Around $T_{\mathrm{ice}} + 3$ K, the weight percentage of HNO_3 in the H_2O/H_2SO_4/HNO_3 droplets (also termed supercooled ternary solution, STS, droplets) exceeds that of H_2SO_4 (Carslaw et al., 1994). This temperature is called T_{STS}, below which particle volume increases significantly. The STS droplet median radius increases to around 300 nm (Jumelet et al., 2008) and the effective radius to 400 nm at these aerosol background conditions. The surface area increases by a factor of around 10 compared to the one for the SBS size distribution.

https://doi.org/10.5194/acp-2022-247
Preprint. Discussion started: 12 April 2022


Atmospheric Chemistry and Physics Discussions

Figure 2 illustrates the transition from the background aerosol droplets to the PSC liquid droplets. Our focus is on the liquid PSC particles. Heterogeneous chlorine and bromine activation takes place to about 90% on the surface of the STS droplets (Carslaw et al., 1994; Kawa et al., 1997; Solomon, 1999; Wegner et al., 2012; Kirner et al., 2015), much less on NAT (nitric acid trihydrate) and ice particles. Extensive chemical loss of polar O_3 in both hemispheres is, however, always accompanied by an extensive removal of HNO_3 (denitrification) by the gravitational settling of NAT particles that are able to grow to large sizes (Solomon, 1999; Fahey et al., 1990, 2001). Dehydration moderates chemical loss of polar ozone as well. Efficient dehydration results from gravitational settling of ice cyrstals (Tritscher et al., 2021).

The sketch in Fig. 2 also indicates the inclusion of insoluble meteoritic particle fragments in the SBS and STS droplets by small dots. The particle number concentration of the liquid PSC particles forming from the SBS particles remain at the low number concentrations of 5-10 cm^{-3}. The strong increase of the particle surface area of the PSCs, however, leads to an increase of the halogen activation potential by an order of magnitude compared to background aerosol conditions. Orographic influences (e.g., triggering mountain wave evolution) and specific meteorological features are responsible for the year to year varying PSC characteristics and the strength of the springtime ozone depletion and for the differences between ozone reduction over the Arctic and Antarctica. The PSC volume over Antarctica is about a factor 5-8 higher than over the Arctic (Pitts et al., 2018).

The stratospheric background particles also initiate NAT particle nucleation and ice formation via heterogeneous nucleation on preexisting foreign nuclei such as the meteoritic material (Curtius et al., 2005; Engel et al., 2013; Hoyle et al., 2013). In the presence of ice, NAT nucleation on ice surfaces is suggested to be the most likely nucleation mechanism, however, this is only valid for mountain wave PSCs with extreme NAT supersaturations (Luo et al., 2003). Ice crystals form at temperatures a few degrees below T_{ice}, though ice may form heterogeneously from STS droplets in the presence of ice nuclei such as meteoritic material (Engel et al. 2013). During strong mountain wave events characterized by high cooling rates, PSCs are predominantly formed by homogeneous ice nucleation for which supercooling of about 3–4 K below T_{ice} is required (Carslaw et al., 1998; Dörnbrack and Leutbecher, 2001; Noel et al., 2009). This can be followed by deposition nucleation of NAT on the ice particles (Luo et al., 2003). Heterogeneous ice nucleation on preexisting NAT particles is another reasonable pathway (Koop et al., 1997b; Voigt et al., 2018). Furthermore, Bogdan et al. (2011) showed that fumed silica, possibly representative of meteoritic smoke particles, is suitable for inducing heterogeneous freezing of ice under stratospheric conditions.

2.2 Volcanically perturbed stratosphere

Figure 2 shows how the emission of volcanic sulfate aerosol impacts the STS droplet population. The increase in aerosol particle and PSC particle number concentration is symbolized by three instead of one particle (stratospheric background scenario). It is well documented that volcanic sulfate particles can significantly influence ozone depletion by increasing the particle surface area available for the activation of ozone-destroying halogen components (Hofmann and Solomon, 1989; Portmann et al., 1996; Solomon, 1999; Dhomse et al., 2015). Strong volcanic eruptions inject large amounts of SO_2 into the lower stratosphere. SO_2 is converted to H_2SO_4/H_2O aerosol within the first three months after injection with maximum conversion rate about six weeks

https://doi.org/10.5194/acp-2022-247
Preprint. Discussion started: 12 April 2022


Atmospheric Chemistry and Physics Discussions

after the eruption. Then the volcanic perturbation declines with an e-folding decay time of about 90 days for minor eruptions (Haywood et al., 2010; Bègue et al., 2017) to 14-16 months for major eruptions (Ansmann et al., 1997; Sekiya et al., 2016).

Ozonesonde and satellite observations showed enhanced midlatitude and Antarctic ozone losses following the large volcanic eruptions of Mount Pinatubo in 1991 and El Chichon in 1982 (Hofmann and Oltmans, 1993; Solomon et al., 2005). We documented the impact of the Pinatubo aerosol on ozone depletion in the winter and spring seasons of 1992 and 1993 over NH midlatitudes based on lidar and ozonesonde observations at Leipzig and Lindenberg (53°N), Germany, respectively, and found a maximum ozone loss of 30% in the strongly polluted lower stratosphere characterized by particle surface area concentrations of 25-35 μm^2 cm^{-3} (Ansmann et al., 1996). Recent modeling studies indicated that even minor eruptions such as the eruption of the Chilean Calbuco volcano in April 2015 can cause significant ozone reduction (Solomon et al., 2017; Ivy et al., 2017; Stone et al., 2017; Zhu et al., 2018). This is surprizing because of the rather low contribution to the stratospheric AOT at 532 nm with a maximum value of 0.007 (Bègue et al., 2017), just a factor of 2 more than the stratospheric aerosol background AOT and a factor of 30 less than the maximum Pinatubo-aerosol-related AOT.

In the sketch in Fig. 2 (volcanic aerosol), we assume pure volcanic sulfate particles without any insoluble particle fragments (such as fine ash) (Muser et al., 2020; Zhu et al., 2020), which could contribute to the PSC formation process (NAT and ice nucleation) via heteorogenous nucleation pathways. Sulfate aerosol originating from minor to moderate volcanic eruptions such as the Sarychev (2009), Calbuco (2015), and Raikoke (2019) eruptions shows an accumulation mode with enhanced number concentrations ranging from 20-100 cm^{-3}, a median radius of about 150 nm, and an effective radius around 200 nm (Mattis et al., 2010; Zhu et al., 2018). In contrast, after the major Pinatubo eruption, the particle number concentrations was below 10 cm^{-3}, and the median and effective radius were high with values of 300-400 nm and 400-600 nm, respectively (Ansmann et al., 1997; Deshler et al., 2003). The sketch in Fig. 2 shows the scenario of a minor volcanic eruption with a high particle number concentration (compared to background conditions). When these numerous volcanic particles are involved in PSC formation, the particles may grow up to about 180-250 nm median radius instead of 300 nm (background case). As a consequence, the overall PSC surface area (liquid particles) available for heterogeneous chemical processes may increase by a factor of 1.2-3.5 for particle number concentrations from 20-100 cm^{-3} compared to the background aerosol scenario (10 particles per cm^{-3}). This was demonstrated to be the case after the Calbuco volcanic eruption in 2015 as shown in respective model simulations by Zhu et al. (2018).

2.3 Wildfire-smoke-polluted stratosphere

Figure 2 (bottom panel) shows how wildfire smoke may disturb the STS droplet evolution in PSCs. In contrast to the impact of sulfate aerosol (background and volcanic conditions), our knowledge about the influence of wildfire smoke on ozone depleting is very poor. As mentioned already, neither the physical and chemical properties of the aged stratospheric smoke particles (after traveling around the globe for several months or even years) nor the potential of these aged smoke particles to influence PSCs evolution and change the PSC properties, and thus halogen activation and ozone depletion are well enough understood. The found coincidence of layers with strongly enhanced smoke pollution levels and significant ozone loss was the motivation to elucidate the potential role of smoke particles in more detail.

https://doi.org/10.5194/acp-2022-247
Preprint. Discussion started: 12 April 2022


Atmospheric Chemistry and Physics Discussions

2.3.1 Smoke transport from the fire source to the polar region

Before we focus on the potential impact on the ozone layer, let us briefly review how the smoke is transported from the fire sources to the polar regions. Figure 3 provides a schematic overview of the main smoke lifting and transport pathways from the burning areas up to the stratosphere and then within the stratosphere to the high latitudes. Efficient lifting of fresh fire smoke to the upper troposphere and lower stratosphere via strong pyrocumulonimbus (pyroCb) convection (Fromm et al., 2010) occurs within a short time period of 30-120 minutes. Only a small fraction of the smoke particles serve as cloud condensation nuclei and ice-nucleating particles in the cloud towers and a low amount of precipitation is produced in these cloud towers so that only a small fraction of the smoke is scavenged (Rosenfeld et al., 2007). Most of the smoke particles are exhausted through the anvil to the upper troposphere and lower stratosphere (UTLS).

After entering the lower stratosphere, self-lifting processes cause further ascent of the fire smoke layers (Khaykin et al., 2020; Kablick et al., 2020; Torres et al., 2020; Ohneiser et al., 2020). Smoke particles considerably absorb solar radiation and warm the air masses which then ascend. The potential of smoke to ascend over several months by solar heating is an important aspect that significantly prolongs the residence time of wildfire smoke in the stratosphere (Peterson et al., 2021; Ohneiser et al., 2022). Khaykin et al. (2020) showed that the Australian smoke ascended from 17 to 35 km within 40 days. Ohneiser et al. (2022) reported ascent velocities of 500 m per day of an Australian smoke layer observed over Punta Arenas for more than a week in January 2020. Torres et al. (2020) found ascent rates of 300 m per day for dense Canadian smoke plumes in the NH stratosphere in the summer of 2017.

During the long-term travel around the globe the smoke disperses over all mid and high latitudes within a few weeks as reported for Canadian smoke in 2017-2018 (Baars et al., 2019; Das et al., 2021). The Australian smoke reached Antarctica already at the end of January 2020. A homogeneous layer developed in February-May 2020 (Rieger et al., 2021; Tencé et al., 2022), several months before the polar vortex (illustrated by a filled blue circle in Fig. 3) formed. Smoke particles were observed in the height range from the upper troposphere to about 25 km height for about two years (2020-2021) and thus influenced PSC formation typically taking place between 14 and 24 km height.

In the case of Siberian wildfire smoke in July-August 2019 (involved in ozone depletion over the Arctic in 2020), the smoke reached the UTLS region without the assistance by deep cumulonimbus convection. Self-lifting processes in the middle and upper troposphere caused the smoke to ascend towards the tropopause within several days (Ohneiser et al., 2021).

2.3.2 Chemical composition and aging

A brief summary of known properties of aged smoke is given by Ansmann et al. (2021). Smoke particles from forest fires are largely composed of organic material (organic carbon, OC) and, to a minor part, of black carbon (BC). The BC mass fraction is typically <5% (Dahlkötter et al., 2014; Yu et al., 2019; Torres et al., 2020), Biomass burning aerosol also consists of a complex mixture of organic species including phenolic compounds, organic acids, aromatic molecules, and humic like substances (HULIS) which represent large macromolecules (Lin et al., 2010; Graber and Rudich, 2006; Laskin et al., 2015; Hems et al., 2021). The particles and released vapors within biomass burning plumes undergo chemical and physical aging

https://doi.org/10.5194/acp-2022-247
Preprint. Discussion started: 12 April 2022


Atmospheric Chemistry and Physics Discussions

processes during long-range transport. The original structures of the lifted irregularly shaped carbonaceous particles remain widely unchanged when they enter the dry stratosphere via fast pyroCb lifting (Haarig et al., 2018; Ohneiser et al., 2020). Most of the freshly emitted biomass burning particles are fractal-like aggregates consisting of a BC-containing core with an OC coating (China et al., 2013). After months of travel in the stratosphere, during which the particles undergo further chemical aging and photo-reaction processes (Hems et al., 2021), the smoke particles seem to be compact and spherical (Baars2019, Ohneiser2020). When self-lifting in the troposphere comes into play, aging of smoke (condensation of gases on the smoke particle surfaces) occurs already on the way towards the tropopause. These particles are already compact and spherical in shape before they reach the lower stratosphere (Ohneiser et al., 2021).

At conditions of the UTLS, it can be assumed that the organic species in the biomass burning particles are in a solid (glassy) state (Koop et al., 2011; Shiraiwa et al., 2017; Knopf et al., 2018). The solid phase state is the likely explanation for the long chemical lifetime against multiphase oxidation (Arangio et al., 2015; Knopf et al., 2011; Li et al., 2020; Li and Knopf, 2021). Furthermore, heterogeneous oxidation of glassy organic aerosol particles likely increases their ability to take up water (Slade et al., 2017) and thus contribute to PSC formation and heterogeneous ozone-depleting reactions such as the hydrolysis of N_2O_5 (Solomon et al., 2022). The coated BC particles show most likely a perfect core-shell structure after months to years within the stratosphere as suggested by Dahlkötter et al. (2014). This shape feature is indicated in Fig. 2 (wildfire smoke) by the onion-like structure (black BC core, green OC shell).

2.3.3 Potential smoke impact on PSC formation

Wildfire smoke aerosol also shows an accumulation mode (Ohneiser et al., 2021; Ansmann et al., 2021), with number concentrations in the order of 50-100 cm^{-3}, similar to the Calbuco volcanic aerosol (as symbolized in Fig. 2), and an effective radius of 200 nm, however, sometimes even up to 250-300 nm (Haarig et al., 2018; Ohneiser et al., 2020, 2022). Regarding the pathways of the smoke impact on ozone depletion, we hypothesize the following (as illustrated in Fig. 2): The glassy organic smoke particles are able to serve as sink for H_2O, H_2SO_4, and HNO_3 (via condensation of gases on the particles). We further assume that the smoke particles, if coated with a water or a sulfuric-acid solution, are then able to influence PSC formation processes in the same way as volcanic sulfate aerosol. This approach was also selected by Yu et al. (2021) and supported by Solomon et al. (2022). Several observations corroborate this assumption. Schill et al. (2020) found an increasing fraction of sulfate on smoke particles with increasing residence time in the middle and upper troposphere. Solomon et al. (2022) concluded from a strong decrease of reactive nitrogen species with increasing stratospheric aerosol extinction, caused by the Australian smoke, over southern midlatitudes that hydrolysis of N_2O_5 to form HNO_3 took place on the surface of the smoke particles in a manner that is similar to sulfate particles. A prerequisite for these heterogeneous chemical reactions is that the smoke particles are able to take up water on their surfaces. The open question remains to what extent this assumption, that volcanic sulfate particles and the aged stratospheric smoke particles influence PSC formation in a very similar way, holds in reality. This question needs to be answered in future laboratory work.

For completeness, since the smoke particles are glassy or have at least a solid core part, they may even act as nuclei for NAT and ice crystal formation in PSCs. Under cirrus cloud conditions, solid organic particles can serve as ice-nucleating particles

https://doi.org/10.5194/acp-2022-247
Preprint. Discussion started: 12 April 2022


Atmospheric Chemistry and Physics Discussions

(Murray et al., 2010; Knopf et al., 2018). However, how solid smoke particles impact PSC formation and heterogeneous chemical reactions is not well known and must be clarified in future laboratory and field studies in combination with comprehensive modeling efforts.

3 Aerosol lidar and ozonesonde data

Figure 1 provides an overview of the lidar stations (Polarstern, Punta Arenas) and ozonesonde sites (Ny-Ålesund, Neumayer station, South Pole station). Based on the aerosol and ozone profiles measured at these stations, the impact of smoke on the ozone depletion is analyzed. Also indicated are the major fire regions in central eastern Siberia and Southeastern Australia, the sources for the stratospheric aerosol over the High Arctic and the southern mid- to high latitudes. The most intense fires occurred from mid July to mid August 2019 (Siberian fires) and from 28 December 2019 to 5 January 2020 (Australian fires).

3.1 Aerosol lidar products

Raman lidar observations in the SH were performed at the campus of the University of Magallanes (UMAG) at Punta Arenas (53.2°S, 70.9°W) from November 2018 to November 2021 in the framework of the DACAPO-PESO (Dynamics, Aerosol, Cloud And Precipitation Observations in the Pristine Environment of the Southern Ocean) campaign (Radenz et al., 2021). The main goal of DACAPO-PESO was the investigation of aerosol–cloud interaction processes in rather pristine, unpolluted marine conditions.

As part of the one-year MOSAiC (September 2019 to October 2020), two advanced lidar instruments, a multiwavelength Raman lidar (Engelmann et al., 2021; Ohneiser et al., 2021) and a High Spectral Resolution Lidar (HSRL) (Eloranta, 2005), were operated continuously aboard the drifting German icebreaker Polarstern (Knust, 2017). Both lidar systems are polarization lidars and thus permit detailed monitoring of cloud phase and aerosol morphological features. The ice breaker was trapped in the ice from October 2019 to May 2020 and drifted through the Arctic Ocean at latitudes mainly between 85°N and 88.5°N for seven and a half months (Engelmann et al., 2021). The MOSAiC expedition provided for the first time the unique opportunity to perform lidar observations north of 85°N over the entire winter half year. This part of the Central Arctic is not covered by any regular lidar measurement, neither with ground-based systems nor with the spaceborne CALIPSO lidar which covers latitudes <81.8°N only.

At Punta Arenas as well as aboard Polarstern, multiwavelength Raman lidars of the Polly type (*PO*rtab*L*le *L*idar s*Y*stem) (Engelmann et al., 2016) were used for aerosol profiling (Polly, 2022). The lidar instrument, the measurement channels, and the methods to derive the smoke optical properties such as particle backscatter and extinction coefficient, extinction-to-backscatter ratio (lidar ratio), and linear depolarization ratio were presented in previous publications (Ohneiser et al., 2020, 2021, 2022).

For our study here, we used the 532 nm backscatter coefficients and the measured stratospheric smoke lidar ratios. By multiplying the backscatter coefficients with a characteristic smoke lidar ratio of 85 sr, height profiles of the 532 nm extinction coefficient up to 30 km height were obtained. The extinction coefficients were then converted into particle number and surface-area concentrations by means of a recently introduced conversion scheme for aged stratospheric smoke (Ansmann et al., 2021).

https://doi.org/10.5194/acp-2022-247
Preprint. Discussion started: 12 April 2022


Atmospheric Chemistry and Physics Discussions

Table 1 shows the lidar products and typical uncertainties in the computed values. The derived particle number concentration n_{50} considers the optically active particles with radius >50 nm. Deshler et al. (2003) and Zhu et al. (2018) showed for in-situ measured balloon-borne size distribution considering particles with radius >50 nm that the total particle concentration of the lognormal size distribution (accumulation mode) is underestimated by a factor of about 1.5-2.

As discussed in Ansmann et al. (2021), for aged smoke, a conversion factor of 1.75 Mm $\mu m^2\,cm^{-3}$ was recommended to convert the 532 nm extinction values into surface-area concentrations. This holds for size distributions characterized by effective radii of 220-250 nm. However, we assume that the effective radius shifted towards 200 nm after several months of travel in the stratosphere (as a result of sedimentation and removal of the largest smoke particles). For an effective radius around 200 nm, a conversion factor of 2.5 Mm $\mu m^2\,cm^{-3}$ is more appropriate in the conversion.

In our ozone-related study, we present winter season (PSC season) mean profiles of the particle number and surface area concentration. To obtain these mean profiles, we averaged the available daily backscatter coefficient profiles, in the first step, before we computed the PSC season mean extinction profile and from this, by applying the conversion parameters, the respective mean surface area and particle number concentration n_{50} of the smoke particles. n_{50} considers particles with radius >50 nm.

In Sect. 4.3, we show High Spectral Resolution Lidar (HSRL) observations to corroborate that the persistent stratospheric aerosol layer over the Arctic was a smoke layer and not a volcanic-sulfate-dominated aerosol layer as suggested in several publications (see, e.g., Kloss et al., 2021). The HSRL is part of the ARM (Atmospheric Radiation Measurement) mobile facility AMF-1 (https://www.arm.gov/capabilities/instruments/hsrl) and was operated side by side with the Polly instrument aboard the Polarstern during the MOSAiC expedition. Similar to the Raman lidar Polly, the HSRL system provides vertical profiles of AOT, particle backscatter coefficient, depolarization ratio, and lidar ratio at 532 nm (Eloranta, 2005; HSRL, 2022).

3.2 NDACC ECC ozonesonde profiles

Under the umbrella of NDACC a large number of stations are operated that regularly launch ozonesondes to measure the ozone partial pressure up to about 35 km height. Measurements are performed since more than 30 years. All data in recent decades are from electrochemical concentration cell (ECC) ozonesondes, which have a precision of 3%–5% and an overall uncertainty in ozone concentration of about 10% up to 30 km (Wilka et al., 2021). As shown in Fig. 1, we use the ozone profiles of Ny-Ålesund, Norway (78.9°N, 11.9°E), Neumayer station, Antarctica (70.62°S, 8.37°E), and the South Pole station, Antarctica (90°S). Ozone data are collated by the World Ozone and Ultraviolet Data Centre (WOUDC) (WOUDC, 2022).

The strongest ozone reduction caused by activated chlorine and bromine components occurs during the Arctic spring months of March (Mar) and April (Apr) and the Antarctic spring months of September (Sep) and October (Oct). In order to study the impact of wildfire smoke on ozone depletion over Antarctica, we computed the deviation of the September-October mean ozone profile $O_3(z, \text{Sep-Oct}, y)$ for the years y =2020 and 2021 from the respective long-term (2010-2019) mean ozone profile $O_3(z, \text{Sep-Oct}, 2010\text{-}2019)$. The ozone deviation is given by:

$$\Delta O_3(z, \text{Sep-Oct}, y) = O_3(z, \text{Sep-Oct}, y) - O_3(z, \text{Sep-Oct}, 2010\text{-}2019)\,. \quad (1)$$

https://doi.org/10.5194/acp-2022-247
Preprint. Discussion started: 12 April 2022


Atmospheric Chemistry and Physics Discussions

We used the ozone profiles measured at the Neumayer station and the South Pole station to compute the two-month mean ozone profiles $O_3(z, \text{Sep-Oct}, 2020)$ and $O_3(z, \text{Sep-Oct}, 2021)$ and the long-term mean ozone profile $O_3(z, \text{Sep-Oct}, 2010\text{-}2019)$. The mean (Neumayer + South Pole) ozone profiles represent well the ozone conditions over Antarctica.

In the same way, we computed the two-month mean ozone anomaly from the Ny-Ålesund ozonesonde data in the case of the Arctic ozone hole in 2020:

$$\Delta O_3(z, \text{Mar-Apr}, 2020) = O_3(z, \text{Mar-Apr}, 2020) - O_3(z, \text{Mar-Apr}, 2010\text{-}2019)\,. \tag{2}$$

In order to highlight the record-breaking ozone losses in 2020 on the column ozone values, we calculated the deviation of the profile-mean (0-35 km) and monthly mean ozone particle pressure $O_{3,\text{col}}(m, y)$ from the respective long-term monthly mean (2000-2019):

$$\Delta O_{3,\text{col}}(m, y) = O_{3,\text{col}}(m, y) - O_{3,\text{col}}(m, 2000\text{-}2019)\,. \tag{3}$$

Besides the impact of stratospheric aerosol, the temperature plays an important role in the ozone-destroying processes (Rex et al., 2004; Solomon et al., 2015). The potential to convert reservoir into active halogen species is closely related to the available overall PSC volume (Rex et al., 2004) which, in turn, depends on ambient temperatures. To consider temperature effects on the observed ozone loss, we computed the two-month mean deviation of the stratospheric temperature conditions (and profile structures) during the main PSC seasons (January-February in the Arctic, July-August over Antarctica) for $y =$ 2020 and 2021 from the respective long-term means $T(z, \text{Jan-Feb}, 2010\text{-}2019)$ and $T(z, \text{Jul-Aug}, 2010\text{-}2019)$,

$$\Delta T(z, \text{Jul-Aug}, y) = T(z, \text{Jul-Aug}, y) - T(z, \text{Jul-Aug}, 2010\text{-}2019) \tag{4}$$

and

$$\Delta T(z, \text{Jan-Feb}, 2020) = T(z, \text{Jan-Feb}, 2020) - T(z, \text{Jan-Feb}, 2010\text{-}2019)\,. \tag{5}$$

The temperature profiles were measured together with the ozone partial pressures with the NDACC ozonesondes.

4 Results

4.1 Arctic and Antarctic column ozone anomalies from 2000-2021

Figure 4 provides a first glimpse of the record-breaking ozone depletion over Antarctica and the Arctic in 2020. The monthly mean column ozone anomaly $\Delta O_{3,\text{col}}(m, y)$ from the respective long-term monthly mean (2000-2019) as defined in Eq. (3) is shown. The ozonesonde observations at the Neumayer and South Pole stations are used in Fig. 4a and Ny-Ålesund observations in Fig. 4b. Typical variations in the column mean ozone partial pressure around the climatological monthly mean values are ± 0.5 mPa over Antarctica and ± 1 to ± 2 mPa over the Arctic. A long period with negative ozone anomalies were observed over Antarctica from September 2020 continuously up to the end of 2021. This long period coincides with the strong stratospheric

https://doi.org/10.5194/acp-2022-247
Preprint. Discussion started: 12 April 2022


Atmospheric Chemistry and Physics Discussions

perturbation by wildfire smoke originating from the record-breaking Australian bushfires (Black Summer fires, dark grey area in Fig. 4a) (Ohneiser et al., 2022). The ozone holes in 2020 and 2021 belong to the strongest (regarding ozone reduction) and largest (regarding the covered area with very low ozone amount) observed during the last 40 years (Krummel and Fraser, 2021; Stone et al., 2021).

Two further events of stratospheric aerosol perturbation are indicated by light grey columns in Fig. 4a. The impact of the Chilean Calbuco volcanic eruption in April 2015 caused an ozone anomaly of −0.3 mPa (from the 2010-2019 monthly means, shown as horizontal line) in September and October 2015. The Australian Black Summer wildfires in 2019-2020 led to anomalies of −0.7 to −0.8 mPa. In contrast, the Black Saturday fires in February 2009 (Siddaway and Petelina, 2011) had no impact on the ozone layer (see light grey column from Februray 2009 to December 2009 in Fig. 4a). Compared to the Australian Black Summer smoke pollution level, the Black Saturday aerosol load was an order of magnitude lower (Peterson et al., 2021).

The moderate ozone variations over Antarctica shifted towards positive deviations during the last decade in line with the expected progression of the healing of the Antarctic ozone layer as a consequence of the strong reduction of industrial CFCs (in agreement with the Montreal Protocol) (Stone et al., 2021; Rieger et al., 2021). This shift is indicated by the horizontal line in Fig. 4a.

As shown in Fig. 4b, compared to the Antarctic monthly mean ozone anomalies, the respective ozone deviations from the long-term, climatological monthly means are much stronger over the Arctic (at Ny-Ålesund). Furthermore, a clear trend in the ozone anomalies towards positive values as a result of decreasing CFC levels is not visible in the Arctic ozone data. The largest negative monthly mean ozone deviation of about 3 mPa was observed in March 2020. Wohltmann et al. (2020) reported a near-complete local reduction of Arctic stratospheric ozone. The ozonesonde measurements in the most depleted parts of the polar vortex showed ozone losses up to 93-96% at 18 km height mid of March 2020. Inness et al. (2020) confirmed that ozone columns over large parts of the Arctic reached record low values in March and April 2020. The minimum ozone column value of close to 200 Dobson units (DU) was observed on 18 March 2020.

The Arctic stratosphere was highly polluted with wildfire smoke, mainly from 8 and 18 km height, during the PSC period (January-March 2020). Major Siberian fires occurring in July-August 2019 were most probably responsible for the aerosol burden (Ohneiser et al., 2021). Volcanic aerosol originating from the Raikoke volcanic eruption in June 2019 may have contributed to the stratospheric perturbation by about 10%. The period with strongly enhanced stratospheric aerosol pollution levels (August 2019 to May 2020) is indicated by a dark grey column in Fig. 4b. The light grey column (from August 2017 to May 2018) indicates the period with stratospheric smoke from the Canadian fires in August 2017 (Baars et al., 2019). A noticable impact of the Canadian smoke on ozone depletion is not visible.

https://doi.org/10.5194/acp-2022-247
Preprint. Discussion started: 12 April 2022


Atmospheric Chemistry and Physics Discussions

4.2 Ozone depletion over Antarctica in 2020 and 2021: smoke as the major stratospheric component

4.2.1 OMI observations of spatial ozone anomalies in September and October 2020 and 2021

In Fig. 5, we show the column ozone anomaly pattern over the southern part of the SH in September and October 2020 and 2021. Here we used the Ozone Monitoring Instrument (OMI) on NASA's Aura satellite. The instrument provides daily measurements of total column ozone with a global daily coverage of most of the Earth atmosphere. Note that this satellite product includes both tropospheric and stratospheric ozone. Figure 5 highlights the deviation of the strong ozone hole conditions in 2020 and 2021 from average ozone depletion conditions over Antarctica in September-October 2010-2019. Extraordinarily strong ozone reduction (blue to black colors) was observed over the entire Antarctic continent in October of both years. Krummel and Fraser (2021) emphasized the similarities in the 2020 and 2021 ozone hole metrics that were quite striking regarding size, depth, persistence, and temporal patterns. Fig. 5 corroborates this statement.

Table 2 provides values for the latitudinal (70°-80°S) averaged ozone anomalies in September and October 2020 and 2021. The column ozone values in October 2020 and 2021 deviated by -50 to -60 Dobson units (DU) from the long-term October means, or in relative units by 17-20% from the June mean (2010-2019, 70°-80°S) column ozone amount of 280 DU. The 2010-2019 June ozone values may be regarded as the ozone reservoir available for depletion in September and October. This additional ozone loss of 17-20% is to a large extent linked to the strong stratospheric aerosol perturbation by the Australian bushfire smoke.

The results for 2020 in Table 2 are in good agreement with the findings of Rieger et al. (2021). They discussed column ozone observations in the 13-22 km layer (averaged over the latitudes from 60°-90°S) for the time period from 2012-2020. Negative ozone anomalies of 20-25 DU from the 2012-2019 October column ozone mean value occurred in October 2020. This corresponds to a relative additional ozone depletion of 14-17% (related to the respective 13-22 km column ozone value for June (2012-2019) of around 145 DU).

4.2.2 Vertically and temporally resolved ozone anomalies (2019-2021) over the Neumayer station

Fig. 6 provides a vertically resolved view on ozone depletion in 2020 and 2021. The ozone profiles of the Neumayer station are used. The deviation of each individual ozone sounding, $O_3(z,t)$ at time t, from the long-term monthly mean $O_3(z,m,2010-2019)$ is shown. Base and top heights of the wildfire smoke layer as measured over Punta Arenas (Ohneiser et al., 2022) are given as grey and black circles. We assume that the smoke was homogeneously distributed over the southern part of the SH in the winter of 2020 (about 6 months after smoke injection) so that the observations at the southernmost tip of South America are also representative for the aerosol conditions over the Antarctic continent. This assumption is in good agreement with aerosol extinction observations for the latitudinal belts from 30°S-60°S and from 60°S-90°S presented by Rieger et al. (2021). These authors showed how fast the smoke became distributed over the SH extratropics (30°-90°S). We concluded from their presentations that the smoke extinction values in the 30°-60°S belt were approximately 20% higher than the ones in the 60-90°S zone in June-August 2020 and that the aerosol observations at Punta Arenas at 53.2°S can be regarded to represent well the smoke pollution at the highest southern latitudes.

https://doi.org/10.5194/acp-2022-247
Preprint. Discussion started: 12 April 2022


Atmospheric Chemistry and Physics Discussions

As can be seen, strong negative ozone anomalies (of up to 3-5 mPa partial pressure) are visible between 15 and 23 km height from September-December 2020 and from September-November 2021. Negative ozone deviations (blue colors) dominate in the height range above 14 km from August 2020 to the end of the year 2021. PSCs fully developed in smoke polluted air in both years.

4.2.3 Vertical distributions of smoke properties, ozone and temperature anomalies, and PSCs

We discussed already a potential impact of wildfire smoke on ozone depletion over Antarctica in the spring of 2020 in Ohneiser et al. (2022). In Fig. 7, we continue with our data analysis and extend the discussion to the ozone depletion season in 2021. Aerosol, ozone, temperature, and PSC information is presented. Height profiles of the mean particle surface area (SA) concentration and particle number concentration n_{50} (measured at Punta Arenas) for the winter seasons (June-August 2020 in a, June-August 2021 in d) are shown together with September-October mean ozone deviations from the long term means, computed by using Eq. (1). Neumayer and South Pole ozonesonde data are considered here. PSCs (height ranges in c and f) mainly developed in July and August. The shown frequency of PSC occurrence was retrieved by using the CALIPSO V4 classification scheme (CALIPSO, 2022; Pitts et al., 2009). All CALIOP data for the Southern Hemisphere during the winter seasons 2020 and 2021 were downloaded and the number of PSC entries obtained with the CALIPSO V4 classification were then computed as a function of height. Below 13 km height cirrus clouds are frequently misclassified as PSC, therefore the PSC height range is shown down to 13 km only.

We added temperature deviations from the 2010-2019 mean temperature profiles (Eq. 4) for the July-August period (main PSC season) in Fig. 7c and f. The temperatures were measured with the Neumayer and South Pole ozonesondes. Rex et al. (2004) observed a clear correlation between the overall Arctic PSC volume (area covered by PSCs times vertical extent of the PSC cloud layers) and temperature in the 14–24 km height range and thus a clear link between temperature and ozone loss strength. The modeling studies of Solomon et al. (2015) indicate that a cooling of the polar air mass by 1 K (at temperatures below 192 K) may cause an additional ozone loss in the order of 0.5-1 mPa (Arctic) and around 0.5 mPa (Antarctica) in the 15-20 km height range.

We also indicate stratospheric background aerosol conditions in Fig. 7a and d based on long-term lidar observations at Lauder, New Zealand, from 1992 to 2015 (Sakai et al., 2016). During volcanic quiescent times (unperturbed conditions), particle extinction coefficients at 532 nm wavelength can be as low as 0.1 Mm^{-1} (Sakai et al., 2016; Baars et al., 2019; Ohneiser et al., 2021, 2022) and corresponding minimum stratospheric background AOT values are around 0.0025 and 0.005 for the height ranges from 15-30 km height and from the tropopause (at about 10 km) to 30 km height, respectively. These background extinction levels were converted into SA and n_{50} values (dashed-dotted grey line in Figs. 7a and d) by using conversion factors for typical background sulfate particle size distributions with an effective radius around 0.15 μm (Wandinger et al., 1995; Jäger and Deshler, 2002, 2003).

According to Deshler et al. (2003), the n_{50} values (particle number concentrations considering particles with radius >50 nm only) are a factor of 1.5-2 lower than the total particle number concentration (considering all particles, i.e., also particles with radius <50 nm) at background and perturbed stratospheric conditions. According to the dashed-dotted line in Figs. 7a and d,

https://doi.org/10.5194/acp-2022-247
Preprint. Discussion started: 12 April 2022


Atmospheric Chemistry and Physics Discussions

clean background conditions are characterized by n_{50} values of 2-5 cm^{-3} and SA concentrations of 0.3-1 μm^2 cm^{-3} from 14-23 km height (main PSC height range). These numbers are in good agreement with balloon-borne observations over Laramie (41°N), Wyoming (Deshler et al., 2003) during volcanic quiescent times in the late 1970s (Hofmann and Solomon, 1989) and in the late 1990s (Deshler et al., 2003).

As can be seen in Fig. 7a, the smoke SA concentrations were as high as 10-15 μm^2 cm^{-3} in the 9-12 km height range (below the main PSC height range) over Antarctica in the winter of 2020 and between 1 and 10 μm^2 cm^{-3} in the main PSC region from 14-23 km height and thus roughly an order of magnitude higher than during clean background periods. The particle number concentration n_{50} increased from background values of 2-5 cm^{-3} to 10-50 cm^{-3} in the central PSC height range from 15-20 km. Since the total particle number concentration is about a factor of 1.5-2 higher than the n_{50} values, up to 100 particles per cm^3 were available to influence PSC formations and properties. As discussed in Sect. 2.2 and pointed out by Zhu et al. (2018), a significant increase in PSCc particle number concentrations (STS droplets) can sensitively increase the overall PSC particle surface area concentration.

A pronounced additional ozone loss (Fig. 7b, negative deviation of the September-October ozone concentration from the long-term September-October mean, Eq. 1) was found in the PSC height range in 2020. Since the temperatures in Fig. 7c did not deviate much from the climatological means during the main PSC months July and August in 2020, we hypothesize that this additional ozone loss is exclusively attributed to the exceptionally polluted conditions. The smoke obviously influenced the evolution of PSCs and was thus responsible for the large additional ozone loss in the height range from 14-23 km height via the PSC formation pathway.

In the lower height range (9-12 km height, below the main PSC layer), an expected clear correlation between the smoke SA concentration and an additional ozone loss was, however, not found in 2020. The reason may be related to specific meridional ozone transport and tropospheric-stratospheric exchange processes in 2020. A clear relationship between smoke occurrence and negative ozone anomaly at PSC-free conditions (9-12 km) was found in 2021, only (Fig. 7d-f).

Compared to the winter months of 2020, the smoke particle number and surface area concentrations were lower by a factor of 2 during the next winter season in 2021. However, the values were still a factor of 3-6 above the aerosol background level in 2021. A remarkably clear correlation between the smoke SA and n_{50} concentrations and the additional ozone loss was found for the height range covering the non-PSC layer (9-12 km) as well as the PSC layer (14-24 km). However, this strong additional ozone loss is also correlated with temperature anomalies of -0.6 K to -1 K (14-16 km) and -1 K to -2.6 K (16-23 km). The negative temperature anomalies of, e.g., -0.8 K to -1.8 K in the 15-20 km height range may explain most of the ozone anomaly of around -1 mPa when considering a 0.5 mPa ozone reduction per Kelvin according to the simulations of Solomon et al. (2015). Because a clear knowledge of the temperature impact on ozone loss is missing for Antarctic PSC conditions, it remains an open question to what extent the temperature decrease (compared to the July-August 2010-2019 mean), on the one hand side, and the wildfire smoke impact, on the other hand, contributed to the overall additional ozone loss of 1-2 mPa in the PSC height range. As mentioned above, rather similar ozone hole characteristics were found in both the 2020 and 2021 spring seasons in a clearly smoke-polluted stratosphere. This point will be further discussed in Sect. 4.5.

https://doi.org/10.5194/acp-2022-247
Preprint. Discussion started: 12 April 2022


Atmospheric Chemistry and Physics Discussions

At heights below the PSC layer (9-12 km), especially around the smoke maximum at 12 km height, there is still a remarkable correlation between smoke SA concentration (6-7 μm^2 cm^{-3}) and addition ozone loss of 0.4-1.2 mPa. Temperature effects should be of minor relevance below the PSC height range.

To evaluate the importance of an apparent smoke-related ozone reduction of 0.4-1.2 mPa (9-12 km) and 1-1.5 mPa (15-20 km) the following numbers are useful. Under volcanic widely quiescent stratospheric aerosol conditions (2010-2019) the ozone partial pressure in the central 15-20 km PSC height range dropped from values of 11.5-14.5 mPa (May-June 2010-2019 mean, Neumayer + South Pole stations) to values around 4 mPa (September-October 2010-2019 mean), and thus by 7.5-10.5 mPa (i.e., on average by 65-72%). According to this, a smoke-related further ozone loss of 1-1.5 mPa as found in September-October 2020 corresponds to a relative additional ozone reduction by 10-20%. Regarding ozone depletion in the PSC-free environment (9-12 km), below the PSC layer, the ozonesonde climatologies indicate that the ozone partial pressure dropped, on average (2010-2019), from values of 3-6 mPa to 2-5 mPa. The ozone reduction was typically 0.7-1.2 mPa in the 9-12 km height range in 2010-2019. Thus the additional smoke-related ozone loss of 0.4-1.2 mPa reflects a smoke contribution of 30-50% to the overall 2021 ozone depletion in the 9-12 km height range.

These numbers are in good agreement with Table 2 and also with the study of Rieger et al. (2021). Our analysis of satellite column ozone observations for the latitudinal belt from 70-80°S revealed an additional, smoke-related ozone depletion contribution of 10-17 % in 2020 and 10-20% in 2021. The found consistency between the different studies corroborates also that our two-station study (Neumayer and South Pole) is quite representative for the smoke-related impact on ozone depletion over the entire Antarctic continent. It further demonstrates that the Punta Arenas aerosol observations are appropriate to describe the smoke-related stratospheric aerosol perturbation over Antarctica in 2020 and 2021.

4.3 Ozone depletion over the Arctic in 2020: smoke as the major stratospheric component

4.3.1 Smoke identification by HSRL and Raman lidar observations

A first discussion of a potential impact of the strong stratospheric aerosol perturbation over the Arctic in 2019-2020 on the record-breaking Arctic ozone hole in March-April 2020 was given in Ohneiser et al. (2021). Before we can deepen this discussion, we need to clarify that wildfire smoke was the dominating aerosol component throughout the entire stratospheric aerosol layer up to 18 or even 20 km height. Ohneiser et al. (2021) left the question open whether smoke or sulfate aerosol originating from the Raikoke volcanic eruption (Kloss et al., 2021) was prevailing at heights >13 km. Because of too noisy Polly lidar signals, wildfire smoke could unambiguously be identified up to 13 km height only.

Figure 8 shows the observations with the continuously running HSRL over the Polarstern (85-88.5°N) in January and February 2020 (HSRL, 2022). The smoke layer is clearly visible between 8 and 16 km height (light blue layer, aerosol traces reached up to 20 km height). PSCs developed mainly above 18 km height. Cirrus virga often developed and were typically found between 2-10 km height. Cirrus formation was triggered by heterogeneous ice nucleation on the smoke particles (Engelmann et al., 2021). Artic haze (also in dark red) dominated the lidar backscatter signals in the lowest part of the troposphere (Engelmann et al., 2021).

https://doi.org/10.5194/acp-2022-247
Preprint. Discussion started: 12 April 2022


Atmospheric Chemistry and Physics Discussions

Figure 9 presents a comparison of the Polly lidar (in a) with the HSRL observations (in b, 7-8 February 2020) in terms of particle optical properties. Both lidars were operated side by side aboard the Polarstern vessel during the MOSAiC expedition. The 24 h mean backscatter profile in Figure 9a indicates a pronounced aerosol layer from 8-16 km and enhanced backscatter values (above background) up to 20 km height. By using a rather large vertical signal smoothing length of 4000 m we were able to cover the height range up to 15 km with extinction-to-backscatter ratio (lidar ratio) observations. Polly values of the lidar ratio of around 70 sr (532 nm) and 50 sr (355 nm, not shown here) indicate smoke particles as the main optically active aerosol component. Volcanic particles would produce lidar ratios around 45 sr at both 355 and 532 nm wavelengths (Mattis et al., 2010). The Polly results are corroborated by the HSRL data analysis in Fig. 9b. The height profile of an increasing aerosol optical thickness (AOT, red noisy profile), directly obtained from the measured pure Rayleigh signals, is compared with several AOT profiles obtained by the integration of the measured 532 nm particle backscatter coefficient from 8 km to height z multiplied by a given lidar ratio, which was varied between 20 sr and 80 sr. The best match with the directly observed AOT was found for a typical smoke lidar ratio of 70 sr. This corroborates our general hypothesis that wildfire smoke dominated throughout the entire layer up to 20 km with a 10% Raikoke sulfate contribution (Ohneiser et al., 2021).

4.3.2 Vertically and temporally resolved ozone anomalies (2019-2020) over Ny-Ålesund

The impact of the Siberian wildfire smoke on the formation of the record breaking ozone depletion in the Arctic in the spring of 2020 is visualized in Fig. 10. The deviation $\Delta O_3(z,t)$ of each individual ozone sonde observation $O_3(z,t)$ at time t from the long-term monthly mean ozone partial pressure $O_3(z,m,2010-2019)$ is shown. The ozone profiles of the Arctic Ny-Ålesund ozonesonde station (78.9°N), about 800 km south of the Polarstern during the winter and spring months in 2020, are used here. Base and top heights of the main wildfire smoke layer as measured over the Polarstern during the MOSAiC campaign (Ohneiser et al., 2021) are given in this height-time display as gray and black circles.

As can be seen, negative ozone deviations (blue colors) prevailed since the summer of 2019. Rather strong negative deviations were then measured between 15 and almost 25 km height in March and April 2020. According to Wohltmann et al. (2021), the Arctic stratospheric winter 2019/2020 was the coldest winter ever observed in the Arctic stratosphere and showed the lowest ozone mixing ratios ever measured in the Arctic polar vortex. The vortex-averaged ozone loss was one of the largest ever observed in the Arctic. The strong ozone depletion remained visible (blue colors in the smoke height range) even during the summer of 2020 when meridional ozone transport usually replenished the ozone layer over the Arctic and compensated for the spring time ozone losses. However, obviously ozone depletion occurred over large parts of the NH so that such a replenishment was not possible.

4.3.3 Vertical distributions of smoke properties, ozone and temperature anomalies, and PSCs

In Fig. 11, we present our findings regarding aerosol, ozone, temperature, and PSC conditions over the Arctic, in a similar way as for the Antarctic ozone depletion events in Fig. 7. The smoke layer did almost not overlap with the main PSC layer $>$17 km. The rather strong additional ozone loss of up to 10 mPa around 18 km height over Ny-Ålesund can be easily explained by the extraordinarily strong temperature deviation of -8.5 K from the long-term January-February (2010-2019) mean. However,

https://doi.org/10.5194/acp-2022-247
Preprint. Discussion started: 12 April 2022


Atmospheric Chemistry and Physics Discussions

by using the temperature dependence of about 1 mPa ozone reduction per Kelvin as discussed in Sect. 4.2.3, again a residual ozone loss of 1-2 mPa can be attributed to the smoke occurrence.

A clear impact of smoke is visible in the height range below the PSC region (at 9-12 km height). Surface area concentrations of 6-10 μm^2 cm^{-3} are correlated with an additional ozone loss of 2-3.5 mPa. These values represent an additional ozone reduction of further 50% when related to the November 2010-2019 ozone mean values and 30% when related to the March-April 2010-2019 ozone mean values.

It is interesting to note in this context, that Inness et al. (2020) also found a strong negative ozone anomalies (3-4 mPa) at heights around 10-11 km (200 hPa). Their study was based on Copernicus Atmosphere Monitoring Service (CAMS) reanalysis data (available for the years 2003-2020). Furthermore, Manney et al. (2020) reported MLS (Aura Microwave Limb Sounder) observations and mentioned that chlorine activation and ozone depletion began earlier in 2019 than in any previously observed winter over the Arctic with evidence of chemical ozone loss starting already in November 2019. Active chlorine then persisted as late into spring. Peak chlorine activation, and thus peak ozone loss, occurred at lower altitudes in 2020 than in other years (2003-2020) except during the cold year of 2011.

4.4 Comparisons of Arctic and Antarctic smoke layers

Two summarizing figures are presented in this and the next section. Figure 12 allows a comparison of the stratospheric smoke conditions over the Arctic in 2020 and Antarctica in 2020 and 2021. Very similar layering structures were observed over both polar regions with maximum aerosol values just above the tropopause. The SA concentration and related n_{50} values of the Australian smoke were clearly above the background aerosol level up to 23 km height in June-August 2020 and 2021 so that PSC formation fully occurred in a smoke-polluted environment in the two winter seasons of 2020 and 2021. The PSC height ranges are given in the left part of Fig. 12. In contrast to the SH smoke conditions, the main Siberian smoke layer was found at lower heights, did not overlap much with the main PSC layer, and smoke SA and n_{50} values reached background levels already at about 18 km height.

Several SA values of volcanic sulfate particles are shown for comparison in Fig. 12. The high SA concentrations of 10-20 μm^2 cm^{-3} were observed over northern Germany at 53°N in 1993 during the second winter and spring months after the Pinatubo eruption (Ansmann et al., 1996). In contrast to the first winter (1991-1992), the Pinatubo aerosol was homogeneously distributed over the entire mid and high northern latitudes (up to the North Pole) in the winter of 1992-1993. Values of 1-5 μm^2 cm^{-3} were observed over mid and high southern latitudes several months after the Chilean Calbuco volcano (Bègue et al., 2017; Zhu et al., 2018). Even this minor volcanic eruption causing stratospheric 532 nm AOTs of up to 0.007 (compared to 0.25-0.3 after the Pinatubo eruption) had a noticeable impact on ozone depletion over Antarctica in the spring of 2015 (Solomon et al., 2015; Zhu et al., 2018; Stone et al., 2021).

4.5 Correlation between smoke levels and ozone anomalies

To further illuminate the impact of Australian and Siberian smoke on ozone destruction in the stratosphere, correlations between the smoke SA concentration and the observed additional ozone loss are presented in Fig. 13. The same smoke and ozone data

https://doi.org/10.5194/acp-2022-247
Preprint. Discussion started: 12 April 2022


Atmospheric Chemistry and Physics Discussions

as shown in Figs. 7 and 11 are used. We added two data pairs for volcanic perturbed, PSC-free conditions (big black circles, Calbuco and Pinatubo-related ozone loss values) (Zhu et al., 2018; Ansmann et al., 1996). The Calbuco-related ozon loss was simulated for 70°S in September 2015 and constrained to satellite observations of Calbuco aerosol optical properties (Zhu et al., 2018). In the case of the Pinatubo scenario, we analyzed Ny-Ålesund ozone profile data for March-April 1993 and computed the ozone deviation from the long-term (March-April, 1998-2008) mean ozone profile and interpreted the found negative ozone anomalies as the contribution of Pinatubo volcanic aerosol to the observed ozone loss in the spring of 1993. The volcanic-induced ozone depletion over Ny-Ålesund was very similar to the ozone depletion values observed over Germany (Lindenberg, near Berlin) (Ansmann et al., 1996).

As can be seen in Fig. 13, at heights below the main PSC layer (closed triangles in Fig. 13), we found a clear increase of the additional ozone loss with increasing SA concentration for the Antarctic observations in 2021 and the Arctic observations in 2020, reasonably in line with the influence of the Calbuco and Pinatubo volcanic aerosol in PSC-free air. For the Antarctic observations in 2020, we did not find any correlation for the lowermost stratospheric region. Potential reasons for the uncorrelated behavior were mentioned in Sect. 4.2.3.

A clear impact of the smoke on ozone depletion via the influence on PSC evolution and properties (PSC formation pathway) was found for the Antarctic winter and spring seasons in 2020 (open red triangles in Fig. 13). In the PSC winter of 2020, the temperatures were close to the climatological mean and thus had no significant impact on the additional ozone loss. However, instead of an expected increase of the additional ozone loss with increasing smoke SA and corresponding n_{50} concentration (causing an expected increase in PSC particle SA concentration) we found an almost SA-independent ozone anomaly of 0.8-2 mPa for SA values from 1-10 μm^2 cm^{-3} or, in terms of n_{50}, from about 10 to 100 cm^{-3}. Note, that SA concentrations of close to 1 μm^2 cm^{-3} in Fig. 13 correspond to smoke aerosol levels still a factor of $\geq$3 above stratospheric background level.

The reason for this behavior remains unclear. One could argue that the found n_{50}-independent ozone depletion is the result of the combination of two compensating effects. Because temperature steadily decreases from 13 to 23 km in the winter months, the conditions for the development of PSCs become increasingly favorable with height. The ability of the smoke particles to influence PSC formation most probably increases with increasing favorable conditions for PSC evolution as well. However, this vertically increasing efficacy of smoke particles being involved in PSC formation processes is compensated by the decrease in the smoke burden with height as shown in Fig. 12a so that the overall impact on ozone depletion via the PSC formation pathway seems to be height- or n_{50}-independent. It should be emphasized that this is our hypothesis. Maybe even other compensation and also saturation effects occurred in the complex heterogeneous chemical processes on the PSC particles.

A similar un-correlated behavior between smoke SA concentration and negative ozone anomaly as in 2020 was also found for the 2021 Antarctic data (orange open triangles in Fig. 13). In both years, the particle number concentration n_{50} was significantly above background level (a factor of 4-12 in the winter of 2020, a factor of 3-7 in the winter of 2021). The similarity in the correlation results for 2020 and 2021 suggest that smoke influenced ozone depletion via the PSC formation pathway in both years.

Finally, the Arctic results (open blue triangles in Fig. 13) remain to be briefly discussed. The strong difference to the Antarctic correlation results (open orange and red triangles) provides a clear view on the impact of the Arctic temperature anomalies (of

https://doi.org/10.5194/acp-2022-247
Preprint. Discussion started: 12 April 2022


Atmospheric Chemistry and Physics Discussions

up to 9 K below the long-term 2010-2019 mean in the 15-23 km height range) on ozone reduction of up to 10 mPa. Currently, it is not possible to accurately correct for these temperature effects to estimate the remaining smoke impact on ozone depletion in the PSC height range above 14 km. As mentioned, if we assume a value of 1 mPa ozone pressure decrease per 1 K cooling (Solomon et al., 2015), the drop in temperature by 8.5 K from the long-term mean at 18 km height explains 8.5 mPa of the observed 10 mPa ozone reduction. The remaining 1.5 mPa of ozone loss may then be related to the smoke impact.

5 Conclusion and outlook

Two major fire events in Siberia in July-August 2019 and Australia in December 2019 to January 2020 caused record-breaking stratospheric smoke pollution over both polar regions in 2020. In this study, we presented for the first time, to the best of our knowledge, a systematic study of the impact of wildfire smoke on ozone depletion in the polar stratosphere over the Arctic and Antarctica. The study was the continuation of previous investigations started by Ohneiser et al. (2021, 2022). Our analyses were based on complex height-resolved observations of smoke particle number and surface area concentrations (aboard Polarstern and at Punta Arenas) and Arctic and Antarctic ozone, temperature and PSC profiling as well as on OMI satellite observations of column ozone in the latitudinal belt from 70°-80°S in the winter and spring seasons of 2020 and 2021.

Clear indications for a smoke impact on PSC formation, halogen activation, and ozone depletion was found over Antarctica in the height range $>$ 13 km in the two consecutive years of 2020 and 2021. The data analysis revealed a smoke-related additional ozone loss over high southern latitudes of 1-1.5 mPa (10-20%), independent of the strength of the smoke pollution, i.e., for particle number concentrations from 10-100 cm^{-3} (factor of 3-10 above stratospheric aerosol background level). The extremely unusual atmospheric conditions over the High Arctic in the winter and spring seasons of 2019-2020 with temperature deviations of up to 9 K from the long-term mean made it impossible to properly quantify the impact of wildfire smoke on PSC formation and subsequent ozone depletion at high northern latitudes. Our PSC-related studies suggest that rather strong fire storms (even stronger than the Austrilian fire storms) combined with lifting of thick smoke layers clearly above 20 km may lead to a complete depletion of the ozone layer over Antarctica during the spring season.

Clear indications for an impact of smoke on ozone depletion for PSC-free conditions (9-12 km) were observed as well. Smoke particle surface area (SA) concentrations in the range of 5-10 μm^2 cm^{-3} were correlated with a smoke-related additional ozone loss of 0.4-1.2 mPa (30-50% contribution to the total ozone loss, Antarctica, 2021) and 2-3.5 mPa (also 30-50% contribution to the total ozone loss, Arctic, 2020).

Satellite observations were used to highlight the ozone depletion on a spatial scale. The satellite data, showing the strong smoke-related ozone over entire Antarctica, were in good agreement with the aerosol and ozone profile studies. The derived additional column ozone loss (deviation from the long-term mean) ranged from 26-30 Dobson units (9-10%) in September 2020 and 2021 and 52-57 Dobson units in October 2020 and 2021 in Antarctic latitudinal belt from 70°-80°S.

Our study may be regarded as a first step and a motivation for further studies on the impact of smoke on ozone depletion. This will include airborne in situ observations, remote sensing, laboratory studies as well as atmospheric modeling in this new field of atmospheric science. Many aspects, especially those related to the chemical composition and microphysical and

https://doi.org/10.5194/acp-2022-247
Preprint. Discussion started: 12 April 2022


Atmospheric Chemistry and Physics Discussions

morphological properties of the aged smoke particles (after traveling around the globe over months and even years and known to impact) need to be investigated in detail. The ability of aged smoke particles to influence heterogeneous chemical processes, cirrus and PSC formation is another important topic of investigations. The relevance for these new studies is given by the expectation that extraordinarily strong wildfires as a consequence of climate warming (higher temperatures, longer droughts) may occur more often in the future. There is a clear and strong need to accurately consider the impact of wildfire smoke on ozone depletion in the ozone-layer-healing and future-climate-change debate. The full importance of strong wildfires need to be well considered in upcoming Intergovernmental Panel on Climate Change (IPCC) reports.

6 Data availability

Polly lidar observations (level 0 data, measured signals) are in the PollyNet database (Polly, 2022). All the analysis products are available upon request (info@tropos.de). MOSAiC HSRL data is available at http://www.arm.gov/data. Specific analysis products derived from Polarstern HSRL observations can be obtained on request (eloranta@wisc.edu). Basic HSRL overviews are avialble at HSRL (2022). The ozone and temperature data from regular NDACC ozonesonde launches at Ny-Ålesund, Neumayer and South Pole station can be downloaded at the NDACC website (NDACC, 2021) and are available through the World Ozone and Ultraviolet Data Center (WOUDC, 2022). Satellite ozone observations were downloaded from the OMI data base available at OMI (2022). Finally, CALIOP observations of PSCs were used (CALIPSO, 2022).

7 Author contributions

The paper was written by AA under strong support by KO, AC, DK, EE, and UW. The data analysis was performed by KO, AC, EE, HB, DV, and RE. PS, MR, CJ, BB, and FZ were involved in the DACAPO-PESO campaign at Punta Arenas and took care of all high quality measurements over the entire 3-year campaign. RE, HG, MR, JH, and DA participated in the MOSAiC field observations aboard Polarstern. All coauthors were actively involved in the extended discussions and the elaboration of the final design of the manuscript.

8 Competing interests

The authors declare that they have no conflict of interest.

9 Financial support

The authors acknowledge support through the European Research Infrastructure for the observation of Aerosol, Clouds and Trace Gases ACTRIS under grant agreement no. 654109 and 739530 from the European Union's Horizon 2020 research and innovation programme. The field observations at Punta Arenas were partly funded by the German Science Foundation (DFG) project PICNICC with project number 408008112. This research has been supported by the U.S. National Science Foundation

https://doi.org/10.5194/acp-2022-247
Preprint. Discussion started: 12 April 2022

Atmospheric Chemistry and Physics Discussions

(grant no. AGS-1446286) and the U.S. Department of Energy, Office of Science (BER), Atmospheric System Research (grant no. DE-SC0021034). The Polarstern Polly data was produced as part of the international Multidisciplinary drifting Observatory for the Study of the Arctic Climate (MOSAiC) with the tag MOSAiC20192020 and Project ID AWI_PS122_00.

Acknowledgements. The ozonesondes at NDACC stations of Ny-Ålesund and at the Neumayer stations were launched by the Alfred-Wegener-Institut, Helmholtz-Zentrum für Polar- und Meeresforschung (AWI), Bremerhaven, Germany. NOAA Earth System Research Laboratory, Global Monitoring Division, Boulder, Colorado, U.S.A. is responsible for the South Pole ozonesonde launches. We thank the PIs, Justus Notholt (Ny-Ålesund, Holger Schmithüsen and Peter von der Gathen (Neumayer station), and Bryan Johnson (South Pole station) and all team members involved in carefully performed NDACC ozonesoundings over decades for the unique high-quality ozone data sets. Monthly average ozone values were produced by the NASA Earth Observations team based on data provided by the OMI team. We are grateful to the MOSAiC team and the RV Polarstern crew for their perfect logistical support during the one-year MOSAiC expedition. We further thank the entire MOSAiC research and logistic teams for their enormous efforts of producing the exemplary and uninterrupted MOSAiC dataset. We are also greatful to the entire research team (University Magellan, Leipzig University, TROPOS) to make the three-year DACAOPO-PESO campaign made the event become a big success. Finally, we are grateful to the CALIPSO team for their well-organized easy-to-use internet platforms.

https://doi.org/10.5194/acp-2022-247
Preprint. Discussion started: 12 April 2022

Atmospheric Chemistry and Physics Discussions

References

Abatzoglou, J. T., Williams, A. P., and Barbero, R.: Global emergence of anthropogenic climate change in fire weather indices, Geophys, Res. Lett., 46, 326–336, https://doi.org/10.1029/2018GL080959, 2019.

Ansmann, A., Wagner, F., Wandinger, U., Mattis, I., Görsdorf, U., Dier, H.-D., and Reichardt, J.: Pinatubo aerosol and stratospheric ozone reduction: Observations over central Europe, Journal of Geophysical Research: Atmospheres, 101, 18 775–18 785, https://doi.org/10.1029/96JD01373, 1996.

Ansmann, A., Mattis, I., Wandinger, U., Wagner, F., Reichardt, J., and Deshler, T.: Evolution of the Pinatubo aerosol: Raman lidar observations of particle optical depth, effective radius, mass, and surface area over Central Europe at 53.4°N, Journal of the Atmospheric Sciences, 54, 2630 – 2641, https://doi.org/10.1175/1520-0469(1997)054<2630:EOTPAR>2.0.CO;2, 1997.

Ansmann, A., Baars, H., Chudnovsky, A., Mattis, I., Veselovskii, I., Haarig, M., Seifert, P., Engelmann, R., and Wandinger, U.: Extreme levels of Canadian wildfire smoke in the stratosphere over central Europe on 21–22 August 2017, Atmospheric Chemistry and Physics, 18, 11 831–11 845, https://doi.org/10.5194/acp-18-11831-2018, 2018.

Ansmann, A., Ohneiser, K., Mamouri, R.-E., Knopf, D. A., Veselovskii, I., Baars, H., Engelmann, R., Foth, A., Jimenez, C., Seifert, P., and Barja, B.: Tropospheric and stratospheric wildfire smoke profiling with lidar: mass, surface area, CCN, and INP retrieval, Atmospheric Chemistry and Physics, 21, https://doi.org/10.5194/acp-21-9779-2021, 2021.

Arangio, A. M., Slade, J. H., Berkemeier, T., Pöschl, U., Knopf, D. A., and Shiraiwa, M.: Multiphase chemical kinetics of OH radical uptake by molecular organic markers of biomass burning aerosols: humidity and temperature dependence, surface reaction, and bulk diffusion, The Journal of Physical Chemistry A, 119, 4533–4544, https://doi.org/10.1021/jp510489z, pMID: 25686209, 2015.

Baars, H., Ansmann, A., Ohneiser, K., Haarig, M., Engelmann, R., Althausen, D., Hanssen, I., Gausa, M., Pietruczuk, A., Szkop, A., Stachlewska, I. S., Wang, D., Reichardt, J., Skupin, A., Mattis, I., Trickl, T., Vogelmann, H., Navas-Guzmán, F., Haefele, A., Acheson, K., Ruth, A. A., Tatarov, B., Müller, D., Hu, Q., Podvin, T., Goloub, P., Veselovskii, I., Pietras, C., Haeffelin, M., Fréville, P., Sicard, M., Comerón, A., Fernández García, A. J., Molero Menéndez, F., Córdoba-Jabonero, C., Guerrero-Rascado, J. L., Alados-Arboledas, L., Bortoli, D., Costa, M. J., Dionisi, D., Liberti, G. L., Wang, X., Sannino, A., Papagiannopoulos, N., Boselli, A., Mona, L., D'Amico, G., Romano, S., Perrone, M. R., Belegante, L., Nicolae, D., Grigorov, I., Gialitaki, A., Amiridis, V., Soupiona, O., Papayannis, A., Mamouri, R.-E., Nisantzi, A., Heese, B., Hofer, J., Schechner, Y. Y., Wandinger, U., and Pappalardo, G.: The unprecedented 2017–2018 stratospheric smoke event: decay phase and aerosol properties observed with the EARLINET, Atmospheric Chemistry and Physics, 19, 15 183–15 198, https://doi.org/10.5194/acp-19-15183-2019, 2019.

Bègue, N., Vignelles, D., Berthet, G., Portafaix, T., Payen, G., Jégou, F., Benchérif, H., Jumelet, J., Vernier, J.-P., Lurton, T., Renard, J.-B., Clarisse, L., Duverger, V., Posny, F., Metzger, J.-M., and Godin-Beekmann, S.: Long-range transport of stratospheric aerosols in the Southern Hemisphere following the 2015 Calbuco eruption, Atmospheric Chemistry and Physics, 17, 15 019–15 036, https://doi.org/10.5194/acp-17-15019-2017, 2017.

Bernath, P., Boone, C., and Crouse, J.: Wildfire smoke destroys stratospheric ozone, Science, 375, 1292–1295, https://doi.org/10.1126/science.abm5611, 2022.

Bogdan, A., Molina, M. J., Kulmala, M., MacKenzie, A. R., and Laaksonen, A.: Study of finely divided aqueous systems as an aid to understanding the formation mechanism of polar stratospheric clouds: Case of HNO_3/H_2O and H_2SO_4/H_2O systems, Journal of Geophysical Research, 108, https://doi.org/10.1029/2002JD002605, 2011.

https://doi.org/10.5194/acp-2022-247
Preprint. Discussion started: 12 April 2022

CALIPSO(2022): CALIPSO data, Lidar Level 2 Polar Stratospheric Cloud Mask V1, available at https://www-calipso.larc.nasa.gov/resources/calipso_users_guide/data_summaries/psc/index.php last access: 03 February, 2022.

Carslaw, K. S., Luo, B. P., Clegg, S. L., Peter, T., Brimblecombe, P., and Crutzen, P. J.: Stratospheric aerosol growth and HNO_3 gas phase depletion from coupled HNO_3 and water uptake by liquid particles, Geophysical Research Letters, 21, 2479–2482, https://doi.org/10.1029/94GL02799, 1994.

Carslaw, K. S., Wirth, M., Tsias, A., Luo, B. P., Dörnbrack, A., Leutbecher, M., Volkert, H., Renger, W., Bacmeister, J. T., and Peter, T.: Particle microphysics and chemistry in remotely observed mountain polar stratospheric clouds, Journal of Geophysical Research: Atmospheres, 103, 5785–5796, https://doi.org/10.1029/97JD03626, 1998.

China, S., Mazzoleni, C., Gorkowski, K., Aiken, A. C., and Dubey, M. K.: Morphology and mixing state of individual freshly emitted wildfire carbonaceous particles, Nat Commun., 4, https://doi.org/10.1038/ncomms3122, 2013.

Curtius, J., Weigel, R., Vössing, H.-J., Wernli, H., Werner, A., Volk, C.-M., Konopka, P., Krebsbach, M., Schiller, C., Roiger, A., Schlager, H., Dreiling, V., and Borrmann, S.: Observations of meteoric material and implications for aerosol nucleation in the winter Arctic lower stratosphere derived from in situ particle measurements, Atmospheric Chemistry and Physics, 5, 3053–3069, https://doi.org/10.5194/acp-5-3053-2005, 2005.

Dahlkötter, F., Gysel, M., Sauer, D., Minikin, A., Baumann, R., Seifert, P., Ansmann, A., Fromm, M., Voigt, C., and Weinzierl, B.: The Pagami Creek smoke plume after long-range transport to the upper troposphere over Europe - aerosol properties and black carbon mixing state, Atmospheric Chemistry and Physics, 14, 6111–6137, https://doi.org/10.5194/acp-14-6111-2014, 2014.

Das, S., Colarco, P. R., Oman, L. D., Taha, G., and Torres, O.: The long-term transport and radiative impacts of the 2017 British Columbia pyrocumulonimbus smoke aerosols in the stratosphere, Atmospheric Chemistry and Physics, 21, 12 069–12 090, https://doi.org/10.5194/acp-21-12069-2021, 2021.

DeLand, M. T., Bhartia, P. K., Kramarova, N., and Chen, Z.: OMPS LP observations of PSC variability during the NH 2019–2020 season, Geophysical Research Letters, 47, https://doi.org/10.1029/2020GL090216, 2020.

Deshler, T., Hervig, M. E., Hofmann, D. J., Rosen, J. M., and Liley, J. B.: Thirty years of in situ stratospheric aerosol size distribution measurements from Laramie, Wyoming (41°N), using balloon-borne instruments, Journal of Geophysical Research: Atmospheres, 108, https://doi.org/10.1029/2002JD002514, 2003.

Dhomse, S. S., Chipperfield, M. P., Feng, W., Hossaini, R., Mann, G. W., and Santee, M. L.: Revisiting the hemispheric asymmetry in midlatitude ozone changes following the Mount Pinatubo eruption: A 3-D model study, Geophysical Research Letters, 42, 3038–3047, https://doi.org/10.1002/2015GL063052, 2015.

Dowdy, A. J., Ye, H., Pepler, A., Thatcher, M., Osbrough, S. L., Evans, J. P., Di Virgilio, G., and McCarthy, N.: Future changes in extreme weather and pyroconvection risk factors for Australian wildfires, Sci. Rep., 9, https://doi.org/10.1038/s41598-019-46362-x, 2019.

Dörnbrack, A. and Leutbecher, M.: Relevance of mountain waves for the formation of polar stratospheric clouds over Scandinavia: A 20 year climatology, Journal of Geophysical Research: Atmospheres, 106, 1583–1593, https://doi.org/10.1029/2000JD900250, 2001.

Eloranta, E. E.: High Spectral Resolution Lidar, in LIDAR — Range–resolved optical remote sensing of the atmosphere, Springer, New York (ISBN 0-387-40075-3), 143-163, 2005.

Engel, I., Luo, B. P., Pitts, M. C., Poole, L. R., Hoyle, C. R., Grooß, J.-U., Dörnbrack, A., and Peter, T.: Heterogeneous formation of polar stratospheric clouds – Part 2: Nucleation of ice on synoptic scales, Atmospheric Chemistry and Physics, 13, 10 769–10 785, https://doi.org/10.5194/acp-13-10769-2013, 2013.

https://doi.org/10.5194/acp-2022-247
Preprint. Discussion started: 12 April 2022

Engelmann, R., Kanitz, T., Baars, H., Heese, B., Althausen, D., Skupin, A., Wandinger, U., Komppula, M., Stachlewska, I. S., Amiridis, V., Marinou, E., Mattis, I., Linné, H., and Ansmann, A.: The automated multiwavelength Raman polarization and water-vapor lidar Polly^{XT}: the neXT generation, Atmospheric Measurement Techniques, 9, 1767–1784, https://doi.org/10.5194/amt-9-1767-2016, 2016.

Engelmann, R., Ansmann, A., Ohneiser, K., Griesche, H., Radenz, M., Hofer, J., Althausen, D., Dahlke, S., Maturilli, M., Veselovskii, I., Jimenez, C., Wiesen, R., Baars, H., Bühl, J., Gebauer, H., Haarig, M., Seifert, P., Wandinger, U., and Macke, A.: Wildfire smoke, Arctic haze, and aerosol effects on mixed-phase and cirrus clouds over the North Pole region during MOSAiC: an introduction, Atmospheric Chemistry and Physics, 21, https://doi.org/10.5194/acp-21-13397-2021, 2021.

English, J. M., Toon, O. B., Mills, M. J., and Yu, F.: Microphysical simulations of new particle formation in the upper troposphere and lower stratosphere, Atmospheric Chemistry and Physics, 11, 9303–9322, https://doi.org/10.5194/acp-11-9303-2011, 2011.

Fahey, D., Kelly, K., Kawa, S., Tuck, A. F., Loewenstein, M., Chan, K. R., and Heidt, L. E.: Observations of denitrification and dehydration in the winter polar stratospheres, Nature, 344, 321–324, https://doi.org/10.1038/344321a0, 1990.

Fahey, D. W., Gao, R. S., Carslaw, K. S., Kettleborough, J., Popp, P. J., Northway, M. J., Holecek, J. C., Ciciora, S. C., McLaughlin, R. J., Thompson, T. L., Winkler, R. H., Baumgardner, D. G., Gandrud, B., Wennberg, P. O., Dhaniyala, S., McKinney, K., Peter, T., Salawitch, R. J., Bui, T. P., Elkins, J. W., Webster, C. R., Atlas, E. L., Jost, H., Wilson, J. C., Herman, R. L., Kleinböhl, A., and von König, M.: The detection of large HNO_3-containing particles in the winter Arctic stratosphere, Science, 291, 1026–1031, https://doi.org/10.1126/science.1057265, 2001.

Fasullo, J. T., Rosenbloom, N., Buchholz, R. R., Danabasoglu, G., Lawrence, D. M., and Lamarque, J.-F.: Coupled Climate Responses to Recent Australian Wildfire and COVID-19 Emissions Anomalies Estimated in CESM2, Geophysical Research Letters, 48, e2021GL093 841, https://doi.org/10.1029/2021GL093841, 2021.

Feng, W., Dhomse, S. S., Arosio, C., Weber, M., Burrows, J. P., Santee, M. L., and Chipperfield, M. P.: Arctic Ozone Depletion in 2019/20: Roles of Chemistry, Dynamics and the Montreal Protocol, Geophysical Research Letters, 48, e2020GL091 911, https://doi.org/10.1029/2020GL091911, 2021.

Fromm, M., Lindsey, D. T., Servranckx, R., Yue, G., Trickl, T., Sica, R., Doucet, P., and Godin-Beekmann, S.: The Untold Story of Pyrocumulonimbus, Bulletin of the American Meteorological Society, 91, 1193 – 1210, https://doi.org/10.1175/2010BAMS3004.1, 2010.

Graber, E. R. and Rudich, Y.: Atmospheric HULIS: How humic-like are they? A comprehensive and critical review, Atmospheric Chemistry and Physics, 6, 729–753, https://doi.org/10.5194/acp-6-729-2006, 2006.

Haarig, M., Ansmann, A., Baars, H., Jimenez, C., Veselovskii, I., Engelmann, R., and Althausen, D.: Depolarization and lidar ratios at 355, 532, and 1064 nm and microphysical properties of aged tropospheric and stratospheric Canadian wildfire smoke, Atmospheric Chemistry and Physics, 18, 11 847–11 861, https://doi.org/10.5194/acp-18-11847-2018, 2018.

Haywood, J. M., Jones, A., Clarisse, L., Bourassa, A., Barnes, J., Telford, P., Bellouin, N., Boucher, O., Agnew, P., Clerbaux, C., Coheur, P., Degenstein, D., and Braesicke, P.: Observations of the eruption of the Sarychev volcano and simulations using the HadGEM2 climate model, Journal of Geophysical Research: Atmospheres, 115, https://doi.org/10.1029/2010JD014447, 2010.

Heinold, B., Baars, H., Barja, B., Christensen, M., Kubin, A., Ohneiser, K., Schepanski, K., Schutgens, N., Senf, F., Schrödner, R., Villanueva, D., and Tegen, I.: Important role of stratospheric injection height for the distribution and radiative forcing of smoke aerosol from the 2019/2020 Australian wildfires, Atmospheric Chemistry and Physics Discussions, 2021, 1–20, https://doi.org/10.5194/acp-2021-862, 2021.

Hems, R. F., Schnitzler, E. G., Liu-Kang, C., Cappa, C. D., and Abbatt, J. P.: Aging of atmospheric brown carbon aerosol, ACS Earth and Space Chemistry, 5, 722–748, https://doi.org/10.1021/acsearthspacechem.0c00346, 2021.

https://doi.org/10.5194/acp-2022-247
Preprint. Discussion started: 12 April 2022

Hirsch, E. and Koren, I.: Record-breaking aerosol levels explained by smoke injection into the stratosphere, Science, 371, 1269–1274, https://doi.org/10.1126/science.abe1415, 2021.

Hofmann, D. J. and Oltmans, S. J.: Anomalous Antarctic ozone during 1992: Evidence for Pinatubo volcanic aerosol effects, Journal of Geophysical Research: Atmospheres, 98, 18 555–18 561, https://doi.org/10.1029/93JD02092, 1993.

Hofmann, D. J. and Solomon, S.: Ozone destruction through heterogeneous chemistry following the eruption of El Chichón, Journal of Geophysical Research: Atmospheres, 94, 5029–5041, https://doi.org/10.1029/JD094iD04p05029, 1989.

Hoyle, C. R., Engel, I., Luo, B. P., Pitts, M. C., Poole, L. R., Grooß, J.-U., and Peter, T.: Heterogeneous formation of polar stratospheric clouds – Part 1: Nucleation of nitric acid trihydrate (NAT), Atmospheric Chemistry and Physics, 13, 9577–9595, https://doi.org/10.5194/acp-13-9577-2013, 2013.

HSRL(2022): High Spectral Resolution Lidar data, MOSAiC expedition 2019-2020, available at: http://hsrl.ssec.wisc.edu/by_site/33/custom_netcdf/, last access: 15 February, 2022.

Hu, Q., Goloub, P., Veselovskii, I., Bravo-Aranda, J.-A., Popovici, I. E., Podvin, T., Haeffelin, M., Lopatin, A., Dubovik, O., Pietras, C., Huang, X., Torres, B., and Chen, C.: Long-range-transported Canadian smoke plumes in the lower stratosphere over northern France, Atmospheric Chemistry and Physics, 19, 1173–1193, https://doi.org/10.5194/acp-19-1173-2019, 2019.

Inness, A., Chabrillat, S., Flemming, J., Huijnen, V., Langenrock, B., Nicolas, J., Polichtchouk, I., and Razinger, M.: Exceptionally low Arctic stratospheric ozone in spring 2020 as seen in the CAMS reanalysis, Journal of Geophysical Research: Atmospheres, 125, https://doi.org/10.1029/2020JD033563, 2020.

Ivy, D. J., Solomon, S., Kinnison, D., Mills, M. J., Schmidt, A., and Neely III, R. R.: The influence of the Calbuco eruption on the 2015 Antarctic ozone hole in a fully coupled chemistry-climate model, Geophysical Research Letters, 44, 2556–2561, https://doi.org/10.1002/2016GL071925, 2017.

Jäger, H. and Deshler, T.: Lidar backscatter to extinction, mass and area conversions for stratospheric aerosols based on midlatitude balloonborne size distribution measurements, Geophysical Research Letters, 29, 35–1–35–4, https://doi.org/10.1029/2002GL015609, 2002.

Jäger, H. and Deshler, T.: Correction to "Lidar backscatter to extinction, mass and area conversions for stratospheric aerosols based on midlatitude balloonborne size distribution measurements", Geophysical Research Letters, 30, 35–1, https://doi.org/10.1029/2003GL017189, 2003.

Jumelet, J., Bekki, S., David, C., and Keckhut, P.: Statistical estimation of stratospheric particle size distribution by combining optical modelling and lidar scattering measurements, Atmospheric Chemistry and Physics, 8, 5435–5448, https://doi.org/10.5194/acp-8-5435-2008, 2008.

Kablick, G. P., Allen, D. R., Fromm, M. D., and Nedoluha, G. E.: Australian pyroCb smoke generates synoptic-scale stratospheric anticyclones, Geophysical Research Letters, 47, https://doi.org/10.1029/2020GL088101, 2020.

Kawa, S. R., Newman, P. A., Lait, L. R., Schoeberl, M. R., Stimpfle, R. M., Kohn, D. W., Webster, C. R., May, R. D., Baumgardner, D., Dye, J. E., Wilson, J. C., Chan, K. R., and Loewenstein, M.: Activation of chlorine in sulfate aerosol as inferred from aircraft observations, Journal of Geophysical Research: Atmospheres, 102, 3921–3933, https://doi.org/10.1029/96JD01992, 1997.

Khaykin, S., Legras, B., Bucci, S., Sellitto, P., Isaksen, L., Tencé, L., Bekki, S., Bourassa, A., Rieger, L., Zawada, D., Jumelet, J., and Godin-Beekmann, S.: The 2019/20 Australian wildfires generated a persistent smoke-charged vortex rising up to 35 km altitude, Nature Communications Earth and Environment, https://doi.org/10.1038/s43247-020-00022-5, 2020.

https://doi.org/10.5194/acp-2022-247
Preprint. Discussion started: 12 April 2022

Khaykin, S. M., Godin-Beekmann, S., Hauchecorne, A., Pelon, J., Ravetta, F., and Keckhut, P.: Stratospheric Smoke With Unprecedentedly High Backscatter Observed by Lidars Above Southern France, Geophysical Research Letters, 45, 1639–1646, https://doi.org/10.1002/2017GL076763, 2018.

Kirner, O., Müller, R., Ruhnke, R., and Fischer, H.: Contribution of liquid, NAT and ice particles to chlorine activation and ozone depletion in Antarctic winter and spring, Atmospheric Chemistry and Physics, 15, 2019–2030, https://doi.org/10.5194/acp-15-2019-2015, 2015.

Kloss, C., Berthet, G., Sellitto, P., Ploeger, F., Taha, G., Tidiga, M., Eremenko, M., Bossolasco, A., Jégou, F., Renard, J.-B., and Legras, B.: Stratospheric aerosol layer perturbation caused by the 2019 Raikoke and Ulawun eruptions and their radiative forcing, Atmospheric Chemistry and Physics, 21, 535–560, https://doi.org/10.5194/acp-21-535-2021, 2021.

Knopf, D. A., Forrester, S. M., and Slade, J. H.: Heterogeneous oxidation kinetics of organic biomass burning aerosol surrogates by O_3, NO_2, N_2O_5, and NO_3, Phys. Chem. Chem. Phys., 13, 21 050–21 062, https://doi.org/10.1039/C1CP22478F, 2011.

Knopf, D. A., Alpert, P. A., and Wang, B.: The role of organic aerosol in atmospheric ice nucleation: a review, ACS Earth and Space Chemistry, 2, 168–202, https://doi.org/10.1021/acsearthspacechem.7b00120, 2018.

Knust, R.: Polar Research and Supply Vessel POLARSTERN operated by the Alfred-Wegener-Institute, Journal of large-scale research facilities JLSRF, 3, A119, https://doi.org/10.17815/jlsrf-3-163, 2017.

Koop, T. and Carslaw, K. S.: Melting of H_2SO_4 & $4H_2O$ particles upon cooling: implications for polar stratospheric clouds, Science, 272, 1638–1641, https://doi.org/10.1126/science.272.5268.1638, 1996.

Koop, T., Carslaw, K. S., and Peter, T.: Thermodynamic stability and phase transitions of PSC particles, Geophysical Research Letters, 24, 2199–2202, https://doi.org/10.1029/97GL02148, 1997.

Koop, T., Luo, B., Biermann, U. M., Crutzen, P. J., and Peter, T.: Freezing of $HNO_3/H_2SO_4/H_2O$ solutions at stratospheric temperatures: nucleation statistics and experiments, The Journal of Physical Chemistry A, 101, 1117–1133, https://doi.org/10.1021/jp9626531, 1997b.

Koop, T., Bookhold, J., Shiraiwa, M., and Pöschl, U.: Glass transition and phase state of organic compounds: dependency on molecular properties and implications for secondary organic aerosols in the atmosphere, Phys. Chem. Chem. Phys., 13, 19 238–19 255, https://doi.org/10.1039/C1CP22617G, 2011.

Krummel, P. and Fraser, P.: The 2021 Antarctic ozone hole report #12, Climate Science Centre, CSIRO Oceans and Atmosphere, Aspendale, Victoria, https://www.awe.gov.au/sites/default/files/documents/2021-aoh-report-12.pdf, 2021.

Laskin, A., Laskin, J., and Nizkorodov, S. A.: Chemistry of atmospheric brown carbon, Chemical Reviews, 115, 4335–4382, https://doi.org/10.1021/cr5006167, pMID: 25716026, 2015.

Li, J. and Knopf, D. A.: Representation of multiphase OH oxidation of amorphous organic aerosol for tropospheric conditions, Environmental Science & Technology, 55, 7266–7275, https://doi.org/10.1021/acs.est.0c07668, pMID: 33974411, 2021.

Li, J., Forrester, S. M., and Knopf, D. A.: Heterogeneous oxidation of amorphous organic aerosol surrogates byO_3, NO_3, and OH at typical tropospheric temperatures, Atmospheric Chemistry and Physics, 20, 6055–6080, https://doi.org/10.5194/acp-20-6055-2020, 2020.

Lin, P., Engling, G., and Yu, J. Z.: Humic-like substances in fresh emissions of rice straw burning and in ambient aerosols in the Pearl River Delta Region, China, Atmospheric Chemistry and Physics, 10, 6487–6500, https://doi.org/10.5194/acp-10-6487-2010, 2010.

Liu, Y., Stanturf, J. A., and Goodrick, S. L.: Trends in global wild-fire potential in a changing climate, Forest Ecol. Manag., 259, 685–697, https://doi.org/10.1016/j.foreco.2009.09.002, 2009.

Liu, Y., Goodrick, S., and Heilman, W.: Wild-land fire emissions, carbon, and climate: Wildfire-climate interactions, Forest Ecol. Manag., 317, 80–96, https://doi.org/10.1016/j.foreco.2013.02.020, 2014.

https://doi.org/10.5194/acp-2022-247
Preprint. Discussion started: 12 April 2022

Luo, B. P., Voigt, C., Fueglistaler, S., and Peter, T.: Extreme NAT supersaturations in mountain wave ice PSCs: A clue to NAT formation, Journal of Geophysical Research: Atmospheres, 108, https://doi.org/10.1029/2002JD003104, 2003.

Manney, G. L., Livesey, N. J., Santee, M. L., Froidevaux, L., Lambert, A., Lawrence, Z. D., Millán, L. F., Neu, J. L., Read, W. G., Schwartz, M. J., and Fuller, R. A.: Record-low Arctic stratospheric ozone in 2020: MLS observations of chemical processes and comparisons with previous extreme winters, Geophysical Research Letters, 47, https://doi.org/10.1029/2020GL089063, 2020.

Mattis, I., Siefert, P., Müller, D., Tesche, M., Hiebsch, A., Kanitz, T., Schmidt, J., Finger, F., Wandinger, U., and Ansmann, A.: Volcanic aerosol layers observed with multiwavelength Raman lidar over central Europe in 2008–2009, Journal of Geophysical Research: Atmospheres, 115, https://doi.org/10.1029/2009JD013472, 2010.

Murray, B. J., Wilson, T. W., Dobbie, S., and Cui, Z.: Heterogeneous nucleation of ice particles on glassy aerosols under cirrus conditions, Nature Geoscience, 3, 233–237, https://doi.org/10.1038/ngeo817, 2010.

Muser, L. O., Hoshyaripour, G. A., Bruckert, J., Horvath, A., Malinina, E., Wallis, S., Prata, F. J., Rozanov, A., von Savigny, C., Vogel, H., and Vogel, B.: Particle aging and aerosol–radiation interaction affect volcanic plume dispersion: evidence from the Raikoke 2019 eruption, Atmos. Chem. Phys., 20, 15 015–15 036, https://doi.org/10.5194/acp-20-15015-2020, 2020.

NDACC(2021): Network for the Detection of Atmospheric Composition Change, ozonesonde profiles, available at: http://www.ndaccdemo.org/, last access: 15 February, 2022.

Noel, V., Hertzog, A., and Chepfer, H.: CALIPSO observations of wave-induced PSCs with near-unity optical depth over Antarctica in 2006–2007, Journal of Geophysical Research: Atmospheres, 114, https://doi.org/10.1029/2008JD010604, 2009.

Ohneiser, K., Ansmann, A., Baars, H., Seifert, P., Barja, B., Jimenez, C., Radenz, M., Teisseire, A., Floutsi, A., Haarig, M., Foth, A., Chudnovsky, A., Engelmann, R., Zamorano, F., Bühl, J., and Wandinger, U.: Smoke of extreme Australian bushfires observed in the stratosphere over Punta Arenas, Chile, in January 2020: optical thickness, lidar ratios, and depolarization ratios at 355 and 532 nm, Atmospheric Chemistry and Physics, 20, 8003–8015, https://doi.org/10.5194/acp-20-8003-2020, 2020.

Ohneiser, K., Ansmann, A., Chudnovsky, A., Engelmann, R., Ritter, C., Veselovskii, I., Baars, H., Gebauer, H., Griesche, H., Radenz, M., Hofer, J., Althausen, D., Dahlke, S., and Maturilli, M.: The unexpected smoke layer in the High Arctic winter stratosphere during MOSAiC 2019–2020, Atmospheric Chemistry and Physics, 21, 15 783–15 808, https://doi.org/10.5194/acp-21-15783-2021, 2021.

Ohneiser, K., Ansmann, A., Kaifler, B., Chudnovsky, A., Barja, B., Knopf, D. A., Kaifler, N., Baars, H., Seifert, P., Villanueva, D., Jimenez, C., Radenz, M., Engelmann, R., Veselovskii, I., and Zamorano, F.: Australian wildfire smoke in the stratosphere: the decay phase in 2020/21 and impact on ozone depletion, Atmospheric Chemistry and Physics Discussions, 2022, 1–41, https://doi.org/10.5194/acp-2021-1097, 2022.

OMI(2022): Ozone Monitoring Instrument, available at: https://neo.gsfc.nasa.gov/view.php?datasetId=AURA_OZONE_M and https://acdisc.gesdisc.eosdis.nasa.gov/data/Aura_OMI_Level3/OMTO3e.003/, last access: 15 February, 2022.

Peterson, D. A., Campbell, J. R., Hyer, E. J., Fromm, M. D., Kablick, G. P., Cossuth, J. H., and DeLand, M. T.: Wildfire-driven thunderstorms cause a volcano-like stratospheric injection of smoke, npj Clim Atmos Sci, https://doi.org/10.1038/s41612-018-0039-3, 2018.

Peterson, D. A., Fromm, M. D., McRae, R. H. D., Campbell, J. R., Hyer, E. J., Taha, G., Camacho, C. P., Kablick, G. P., Schmidt, C. C., and DeLand, M. T.: Australia's Black Summer pyrocumulonimbus super outbreak reveals potential for increasingly extreme stratospheric smoke events, npj Clim Atmos Sci, https://doi.org/10.1038/s41612-021-00192-9, 2021.

Pitts, M. C., Poole, L. R., and Thomason, L. W.: CALIPSO polar stratospheric cloud observations: second-generation detection algorithm and composition discrimination, Atmospheric Chemistry and Physics, 9, 7577–7589, https://doi.org/10.5194/acp-9-7577-2009, 2009.

https://doi.org/10.5194/acp-2022-247
Preprint. Discussion started: 12 April 2022

Pitts, M. C., Poole, L. R., and Gonzalez, R.: Polar stratospheric cloud climatology based on CALIPSO spaceborne lidar measurements from 2006 to 2017, Atmospheric Chemistry and Physics, 18, 10 881–10 913, https://doi.org/10.5194/acp-18-10881-2018, 2018.

Polly(2022): PollyNET lidar data base, available at: http://polly.tropos.de/, last access: 10 January, 2022.

Portmann, R. W., Solomon, S., Garcia, R. R., Thomason, L. W., Poole, L. R., and McCormick, M. P.: Role of aerosol variations in anthropogenic ozone depletion in the polar regions, Journal of Geophysical Research: Atmospheres, 101, 22 991–23 006, https://doi.org/10.1029/96JD02608, 1996.

Radenz, M., Bühl, J., Seifert, P., Baars, H., Engelmann, R., Barja González, B., Mamouri, R.-E., Zamorano, F., and Ansmann, A.: Hemispheric contrasts in ice formation in stratiform mixed-phase clouds: disentangling the role of aerosol and dynamics with ground-based remote sensing, Atmospheric Chemistry and Physics, 21, 17 969–17 994, https://doi.org/10.5194/acp-21-17969-2021, 2021.

Rex, M., Salawitch, R. J., von der Gathen, P., Harris, N. R. P., Chipperfield, M. P., and Naujokat, B.: Arctic ozone loss and climate change, Geophysical Research Letters, 31, https://doi.org/doi.org/10.1029/2003GL018844, 2004.

Rieger, L. A., Randel, W. J., Bourassa, A. E., and Solomon, S.: Stratospheric temperature and ozone anomalies associated with the 2020 Australian New Year fires, Geophysical Research Letters, 48, https://doi.org/10.1029/2021GL095898, 2021.

Rosenfeld, D., Fromm, M., Trentmann, J., Luderer, G., Andreae, M. O., and Servranckx, R.: The Chisholm firestorm: observed microstructure, precipitation and lightning activity of a pyro-cumulonimbus, Atmospheric Chemistry and Physics, 7, 645–659, https://doi.org/10.5194/acp-7-645-2007, 2007.

Sakai, T., Uchino, O., Nagai, T., Liley, B., Morino, I., and Fujimoto, T.: Long-term variation of stratospheric aerosols observed with lidars over Tsukuba, Japan, from 1982 and Lauder, New Zealand, from 1992 to 2015, Journal of Geophysical Research: Atmospheres, 121, 10,283–10,293, https://doi.org/10.1002/2016JD025132, 2016.

Schill, G. P., Froyd, K. D., Bian, H., Kupc, A., Williamson, C., Brock, C. A., Ray, E., Hornbrook, R. S., Hills, A. J., Apel, E. C., Chin, M., Colarco, P. R., and Murphy, D. M.: Widespread biomass burning smoke throughout the remote troposphere, Nat. Geosci., 13, 422–427, https://doi.org/10.1038/s41561-020-0586-1, 2020.

Sekiya, T., Sudo, K., and Nagai, T.: Evolution of stratospheric sulfate aerosol from the 1991 Pinatubo eruption: Roles of aerosol microphysical processes, Journal of Geophysical Research: Atmospheres, 121, 2911–2938, https://doi.org/10.1002/2015JD024313, 2016.

Shiraiwa, M., Li, Y., Tsimpidi, A. P., Karydis, V. A., Berkemeier, T., Pandis, S. N., Lelieveld, J., Koop, T., and Pöschl, U.: Global distribution of particle phase state in atmospheric secondary organic aerosols, Nature Communications, 8, 15 002, https://doi.org/10.1038/ncomms15002, 2017.

Siddaway, J. M. and Petelina, S. V.: Transport and evolution of the 2009 Australian Black Saturday bushfire smoke in the lower stratosphere observed by OSIRIS on Odin, Journal of Geophysical Research: Atmospheres, 116, https://doi.org/10.1029/2010JD015162, 2011.

Slade, J. H., Shiraiwa, M., Arangio, A., Su, H., Pöschl, U., Wang, J., and Knopf, D. A.: Cloud droplet activation through oxidation of organic aerosol influenced by temperature and particle phase state, Geophysical Research Letters, 44, 1583–1591, https://doi.org/10.1002/2016GL072424, 2017.

Solomon, S.: Stratospheric ozone depletion: A review of concepts and history, Reviews of Geophysics, 37, 275–316, https://doi.org/10.1029/1999RG900008, 1999.

Solomon, S., Portmann, R. W., Sasaki, T., Hofmann, D. J., and Thompson, D. W. J.: Four decades of ozonesonde measurements over Antarctica, Journal of Geophysical Research: Atmospheres, 110, https://doi.org/10.1029/2005JD005917, 2005.

Solomon, S., Kinnison, D., Bandoro, J., and Garcia, R.: Simulation of polar ozone depletion: An update, Journal of Geophysical Research: Atmospheres, 120, 7958–7974, https://doi.org/10.1002/2015JD023365, 2015.

https://doi.org/10.5194/acp-2022-247
Preprint. Discussion started: 12 April 2022

Solomon, S., Ivy, D. J., Kinnison, D., Mills, M. J., Neely, R. R., and Schmidt, A.: Emergence of healing in the Antarctic ozone layer, Science, 310, 269–274, https://doi.org/10.1126/science.aae0061, 2017.

Solomon, S., Dube, K., Stone, K., Yu, P., Kinnison, D., Toon, O. B., Strahan, S. E., Rosenlof, K. H., Portmann, R., Davis, S., Randel, W., Bernath, P., Boone, C., Bardeen, C. G., Bourassa, A., Zawada, D., and Degenstein, D.: On the stratospheric chemistry of midlatitude wildfire smoke, Proceedings of the National Academy of Sciences, 119, e2117325 119, https://doi.org/10.1073/pnas.2117325119, 2022.

Stocker, M., Ladstädter, F., and Steiner, A.: Observing the climate impact of large wildfires on stratospheric temperature, Nature Scientific Reports, https://doi.org/10.1038/s41598-021-02335-7, 2021.

Stone, K. A., Solomon, S., Kinnison, D. E., Pitts, M. C., Poole, L. R., Mills, M. J., Schmidt, A., Neely III, R. R., Ivy, D., Schwartz, M. J., Vernier, J.-P., Johnson, B. J., Tully, M. B., Klekociuk, A. R., König-Langlo, G., and Hagiya, S.: Observing the Impact of Calbuco Volcanic Aerosols on South Polar Ozone Depletion in 2015, Journal of Geophysical Research: Atmospheres, 122, 11,862–11,879, https://doi.org/10.1002/2017JD026987, 2017.

Stone, K. A., Solomon, S., Kinnison, D. E., and Mills, M. J.: On recent large Antarctic ozone holes and ozone recovery metrics, Geophysical Research Letters, 48, https://doi.org/10.1029/2021GL095232, 2021.

Tencé, F., Jumelet, J., Bekki, S., Khaykin, S., Sarkissian, A., and Keckhut, P.: Australian Black Summer smoke observed by lidar at the French Antarctic station Dumont d'Urville, Journal of Geophysical Research: Atmospheres, 127, e2021JD035 349, https://doi.org/10.1029/2021JD035349, 2022.

Torres, O., Jethva, H., Ahn, C., Jaross, G., and Loyola, D. G.: TROPOMI aerosol products: evaluation and observations of synoptic-scale carbonaceous aerosol plumes during 2018–2020, Atmospheric Measurement Techniques, 13, 6789–6806, https://doi.org/10.5194/amt-13-6789-2020, 2020.

Tritscher, I., Pitts, M. C., Poole, L. R., Alexander, S. P., Cairo, F., Chipperfield, M. P., Grooß, J.-U., Höpfner, M., Lambert, A., Luo, B., Molleker, S., Orr, A., Salawitch, R., Snels, M., Spang, R., Woiwode, W., and Peter, T.: Polar stratospheric clouds: satellite observations, processes, and role in ozone depletion, Reviews of Geophysics, 59, https://doi.org/10.1029/2020RG000702, 2021.

Voigt, C., Dörnbrack, A., Wirth, M., Groß, S. M., Pitts, M. C., Poole, L. R., Baumann, R., Ehard, B., Sinnhuber, B.-M., Woiwode, W., and Oelhaf, H.: Widespread polar stratospheric ice clouds in the 2015–2016 Arctic winter – implications for ice nucleation, Atmospheric Chemistry and Physics, 18, 15 623–15 641, https://doi.org/10.5194/acp-18-15623-2018, 2018.

Voosen, P.: High-flying wildfire smoke poses potential threat to ozone layer, Science, 374, 921–922, https://doi.org/10.1126/science.acx9655, 2021.

Wandinger, U., Ansmann, A., Reichardt, J., and Deshler, T.: Determination of stratospheric aerosol microphysical properties from independent extinction and backscattering measurements with a Raman lidar, Applied Optics, 34, 8315, https://doi.org/10.1364/AO.34.008315, 1995.

Weber, M., Arosio, C., Coldewey-Egbers, M., Fioletov, V., Frith, S. M., Wild, J. D., Tourpali, K., Burrows, J. P., and Loyola, D.: Global total ozone recovery trends derived from five merged ozone datasets, Atmospheric Chemistry and Physics Discussions, 2022, 1–26, https://doi.org/10.5194/acp-2021-1058, 2022.

Wegner, T., Grooß, J.-U., von Hobe, M., Stroh, F., Sumińska-Ebersoldt, O., Volk, C. M., Hösen, E., Mitev, V., Shur, G., and Müller, R.: Heterogeneous chlorine activation on stratospheric aerosols and clouds in the Arctic polar vortex, Atmospheric Chemistry and Physics, 12, 11 095–11 106, https://doi.org/10.5194/acp-12-11095-2012, 2012.

https://doi.org/10.5194/acp-2022-247
Preprint. Discussion started: 12 April 2022

Weigel, R., Volk, C. M., Kandler, K., Hösen, E., Günther, G., Vogel, B., Grooß, J.-U., Khaykin, S., Belyaev, G. V., and Borrmann, S.: Enhancements of the refractory submicron aerosol fraction in the Arctic polar vortex: feature or exception?, Atmospheric Chemistry and Physics, 14, 12 319–12 342, https://doi.org/10.5194/acp-14-12319-2014, 2014.

Wilka, C., Solomon, S., Kinnison, D., and Tarasick, D.: An Arctic ozone hole in 2020 if not for the Montreal Protocol, Atmospheric Chemistry and Physics, 21, 15 771–15 781, https://doi.org/10.5194/acp-21-15771-2021, 2021.

Wohltmann, I., Gathen, P., Lehmann, R., Maturilli, M., Deckelmann, H., Manney, G. L., Davies, J., Tarasick, D., Jepsen, N., Kivi, R., Lyall, N., and Rex, M.: Near-complete local reduction of Arctic stratospheric ozone by severe chemical loss in spring 2020, Geophysical Research Letters, 47, https://doi.org/10.1029/2020GL089547, 2020.

Wohltmann, I., von der Gathen, P., Lehmann, R., Deckelmann, H., Manney, G. L., Davies, J., Tarasick, D., Jepsen, N., Kivi, R., Lyall, N., and Rex, M.: Chemical Evolution of the Exceptional Arctic Stratospheric Winter 2019/2020 Compared to Previous Arctic and Antarctic Winters, Journal of Geophysical Research: Atmospheres, 126, e2020JD034 356, https://doi.org/10.1029/2020JD034356, 2021.

WOUDC(2022): World Ozone and Ultraviolet Data Center, ozonesonde profiles available at: http://www.ndaccdemo.org/, last access: 15 Februray, 2022.

Yu, P., Toon, O. B., Bardeen, C. G., Zhu, Y., Rosenlof, K. H., Portmann, R. W., Thornberry, T. D., Gao, R.-S., Davis, S. M., Wolf, E. T., de Gouw, J., Peterson, D. A., Fromm, M. D., and Robock, A.: Black carbon lofts wildfire smoke high into the stratosphere to form a persistent plume, Science, 365, 587–590, https://doi.org/10.1126/science.aax1748, 2019.

Yu, P., Davis, S. M., Toon, O. B., Portmann, R. W., Bardeen, C. G., Barnes, J. E., Telg, H., Maloney, C., and Rosenlof, K. H.: Persistent stratospheric warming due to 2019–2020 Australian wildfire smoke, Geophysical Research Letters, 48, https://doi.org/10.1029/2021GL092609, 2021.

Zhu, Y., Toon, O. B., Kinnison, D., Harvey, V. L., Mills, M. J., Bardeen, C. G., Pitts, M., Bègue, N., Renard, J.-B., Berthet, G., and Jégou, F.: Stratospheric aerosols, polar stratospheric clouds, and polar ozone depletion after the Mount Calbuco eruption in 2015, Journal of Geophysical Research: Atmospheres, 123, 12,308–12,331, https://doi.org/10.1029/2018JD028974, 2018.

Zhu, Y., Toon, O., Jensen, E., Bardeen, C. G., Mills, M. J., Tolbert, M. A., Yu, P., and Woods, S.: Persisting volcanic ash particles impact stratospheric SO_2 lifetime and aerosol optical properties, Nat. Commun., 11, 80–96, https://doi.org/10.1038/s41467-020-18352-5, 2020.

https://doi.org/10.5194/acp-2022-247
Preprint. Discussion started: 12 April 2022

Atmospheric Chemistry and Physics Discussions

Table 1. Overview of Polly observational products and characteristic (typical) relative uncertainties in the determined and retrieved properties. Basic smoke parameters measured with lidar are the particle backscatter coefficient and lidar ratio at 532 nm wavelengths. From these data, extinction coefficients are calculated and converted to surface area and number concentration profiles of the smoke particles. In addition, the ozone partial pressure measured with NDACC ozonesondes and used in our study is listed.

Parameter	Uncertainty
Particle backscatter coefficient [Mm^{-1} sr^{-1}]	$\leq$10%
Particle lidar ratio [sr]	10-30%
Particle surface-area concentration [μm^2 cm^{-3}]	35%
Particle number concentration (radius >50 nm) [cm^{-3}]	50%
Ozone partial pressure [mPa]	5-10%

Table 2. Monthly mean column ozone anomalies (i.e., deviations from the long-term September and October 2010-2019 mean column ozone values) plus standard deviations for September and October 2020 and 2021. Averaged values for the latitudinal belt from 70°-80°S are given. Relative ozone deviations are related to the respective long-term, monthly mean June (2010-2019, 70°-80°S) column value of 280 Dobson units (DU).

Month	additional ozone loss	rel. additional ozone loss
September 2020	26±14 DU	9±5%
October 2020	52±21 DU	19±8%
September 2021	30±18 DU	11±6%
October 2021	57±28 DU	20±10%

https://doi.org/10.5194/acp-2022-247
Preprint. Discussion started: 12 April 2022

Atmospheric Chemistry and Physics Discussions

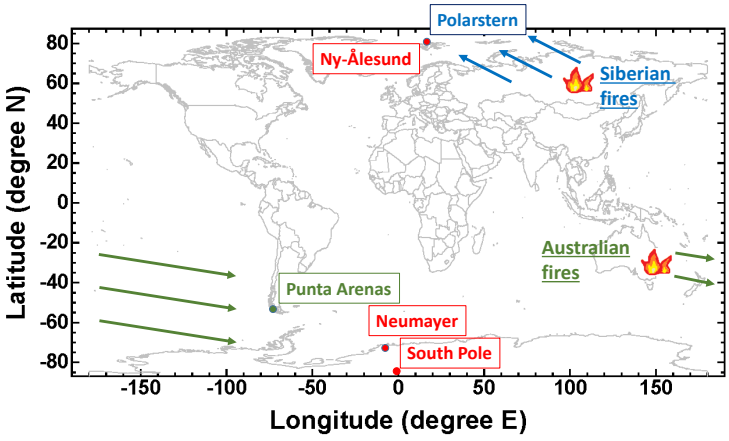

Figure 1. Global map showing the two lidar sites (aboard the icebreaker Polarstern during the one-year MOSAiC expedition and at Punta Arenas in southern Chile during the three-year DACAPO-PESO campaign, explained in Sect. 3.1), the regions with major wildfires (Siberia, Australia), and the ozonesonde sites at Ny-Ålesund, Neumayer, and South Pole station used in the present study. Arrows show the main smoke transport direction towards the Arctic and towards South America and Antarctica during the initial dispersion phase.

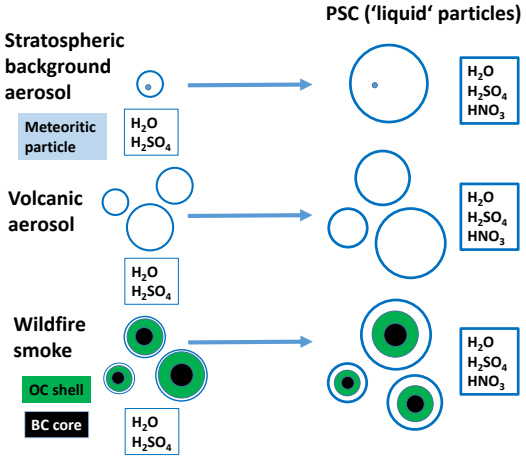

Figure 2. Formation of PSC particles (STS droplets) for three different aerosol scenarios (clean background, volcanic aerosol, wildfire smoke). Three aerosol particles symbolize an increase in aerosol particle number concentration (volcanic and smoke scenarios) which leads to an increased STS droplet number concentration and, on average, smaller STS droplets (compared to background conditions). Insoluble meteoritic particles (small dots, background aerosol) may be immersed within the background sulfate and STS droplets. Smoke particles are shown as BC-core-OC-shell structure with H_20/H_2SO_4 coating (white sphere). By HNO_3 uptake all STS droplets grow to large sizes (see text for more explanations).

https://doi.org/10.5194/acp-2022-247
Preprint. Discussion started: 12 April 2022

Atmospheric Chemistry and Physics Discussions

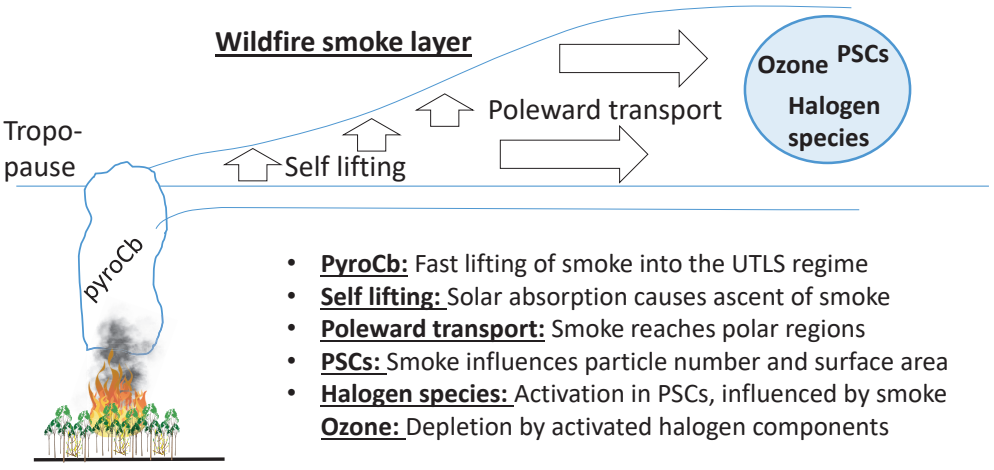

Figure 3. Key processes of the vertical and meridional transport of wildfire smoke from the emission sources to the polar regions.

https://doi.org/10.5194/acp-2022-247
Preprint. Discussion started: 12 April 2022

Atmospheric Chemistry and Physics Discussions

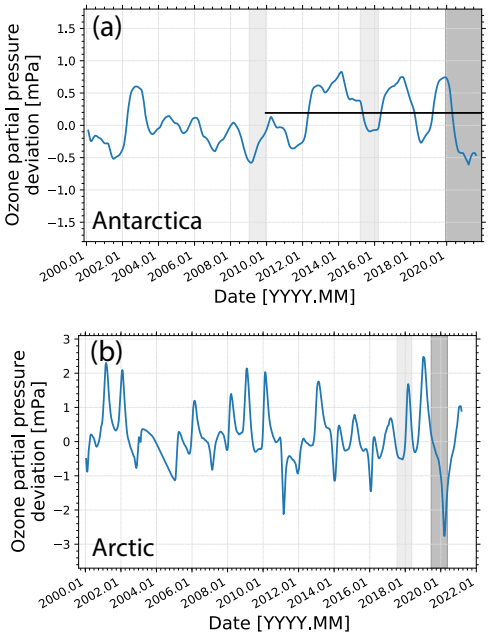

Figure 4. (a) Column ozone anomaly expressed as difference between the monthly mean, vertical mean ozone partial pressure (0-35 km height) from the respective climatological (2000-2019) monthly mean (Eq. 3). Ozone profiles measured at the Antarctic Neumayer and South Pole stations are considered in the top panel. (b) Same as (a), but based on ozone profiling at the Arctic Ny-Ålesund station. Dark grey columns mark the time periods with strong stratospheric aerosol perturbations after the major Australian fire events (Black Summer, in a) and Siberian fires (in b). Light grey columns indicate time periods after the Australian fires in 2009 (Black Saturday, in a) and the Calbuco volcanic eruption in April 2015 (in a), and the Canadian fires (in b, period of influence from August 2017 to January 2018). The horizontal line in (a) emphasizes the change in average ozone level, possibly caused by the healing of the ozone layer during the last years.

https://doi.org/10.5194/acp-2022-247
Preprint. Discussion started: 12 April 2022

Atmospheric Chemistry and Physics Discussions

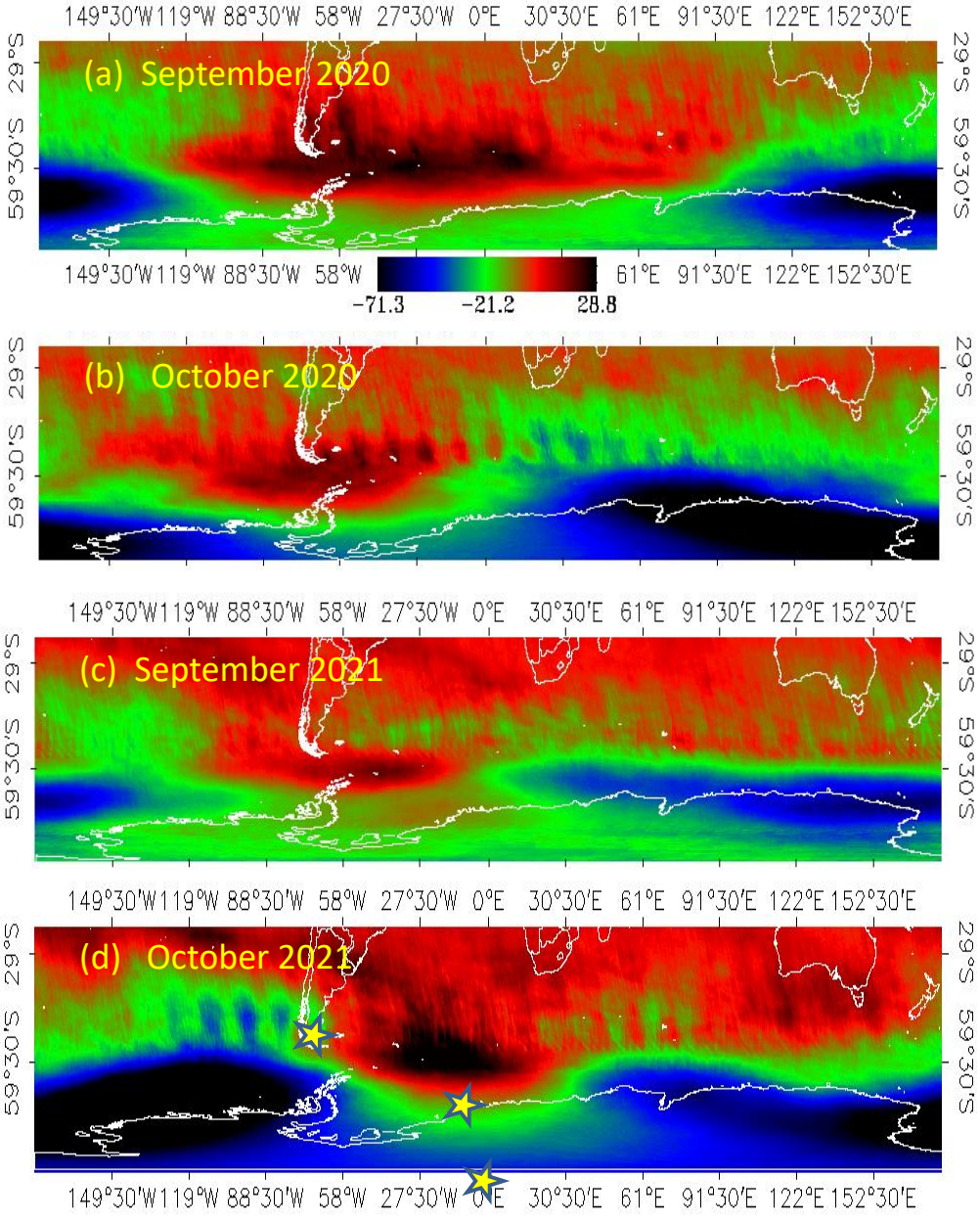

Figure 5. (a,c) September and (b,d) October 2020 and 2021 column ozone deviations (monthly means in Dobson units) from the respective September and October 2010-2019 column ozone means. Observations of the Ozone Monitoring Instrument (OMI) aboard the NASA Aura spacecraft are used (OMI, 2022). Both years are similar regarding the additional ozone loss pattern over Antarctica (green, blue and black colors). In panel d, Punta Arenas (53.2°S), the Neumayer (70.6°N) and the South Pole stations are indicated by yellow stars.

https://doi.org/10.5194/acp-2022-247
Preprint. Discussion started: 12 April 2022

Atmospheric Chemistry and Physics Discussions

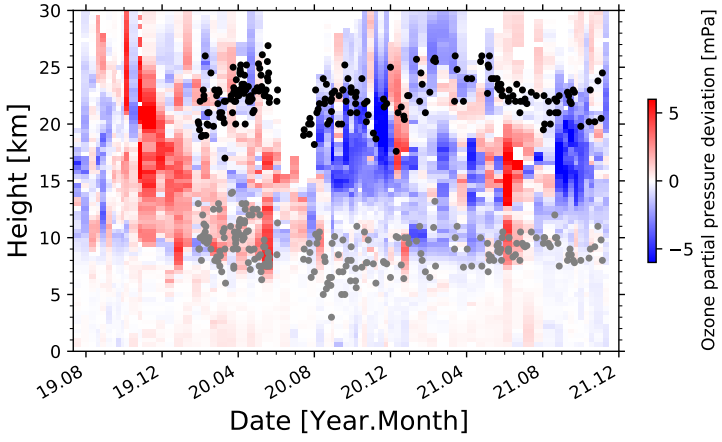

Figure 6. Deviation of each individual ozone profile from the respective long-term (2010-2019) monthly mean ozone profile. Measurements at the Neumayer station (70.6°S) are used. The base (grey dots) and top heights (black dots) of the Australian smoke layer measured with Polly at Punta Arenas on a daily basis indicate the smoke-polluted height range. Gaps in the lidar data after December 2019 are caused by cloudy weather and instrumental problems.

https://doi.org/10.5194/acp-2022-247
Preprint. Discussion started: 12 April 2022

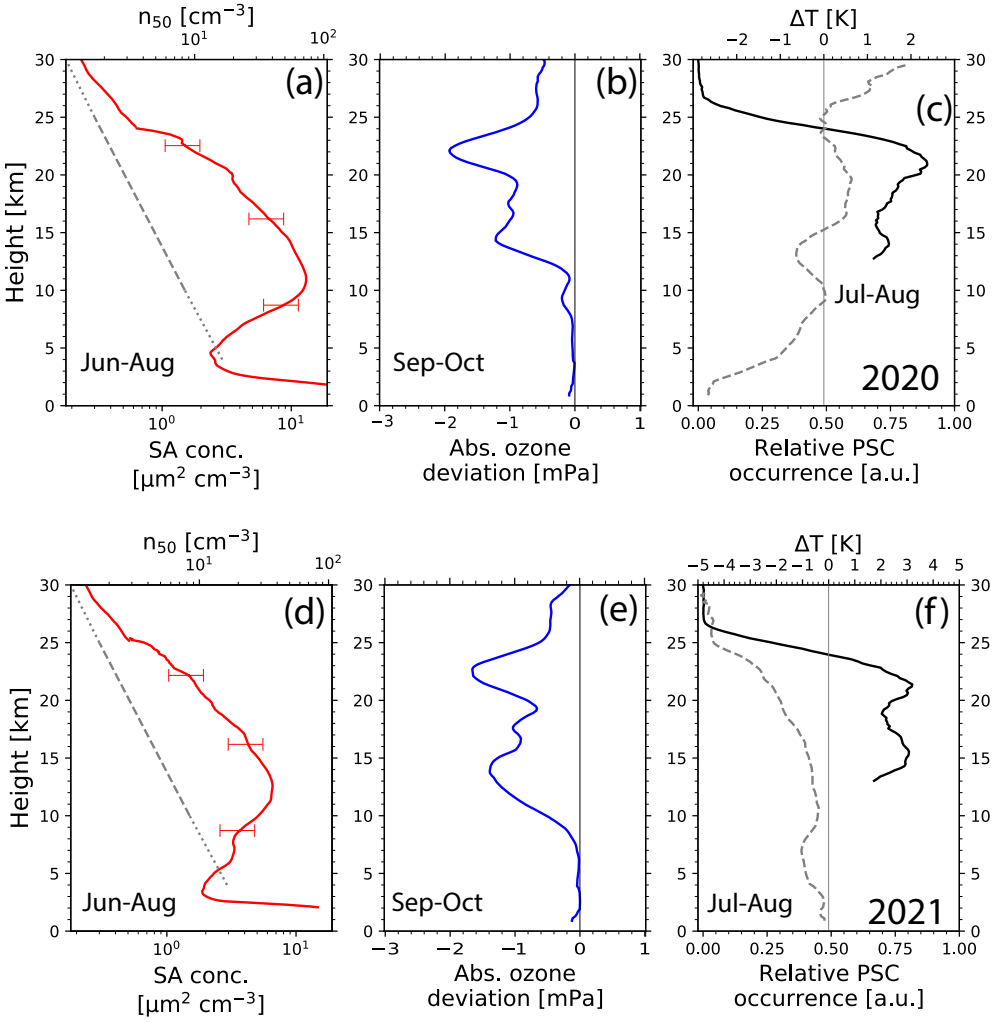

Figure 7. (a) Winter (June-August) mean profiles of the particle surface area (SA) concentration and number concentration n_{50} (particles with radius >50 nm) estimated from lidar observations at Punta Arenas in 2020. Horizontal bars indicate a SA retrieval uncertainty of 35%. Background aerosol estimates are given as a grey dashed line, based on lidar observations at Lauder, New Zealand (Sakai et al., 2016). Dotted line segments indicate extrapolations. (b) Additional ozone loss for September-October 2020, i.e., absolute ozone deviations from the respective long-term September-October (2010-2019) mean profile (see Eq. 1). (c) PSC height range (restricted to heights >13 km) and relative vertical distribution of the PSC frequency of occurrence (in arbitrary units) from CALIOP observations and mean temperature deviations (dashed line) for the main PSC months July-August 2020 from the respective July-August long-term mean profile (calculated with Eq. 4). Ozondesonde data collected at the Neumayer and South Pole stations are used (averaged) in the ozone and temperature calculations. (d)-(f) same as (a)-(c) except for 2021.

https://doi.org/10.5194/acp-2022-247
Preprint. Discussion started: 12 April 2022

Atmospheric Chemistry and Physics Discussions

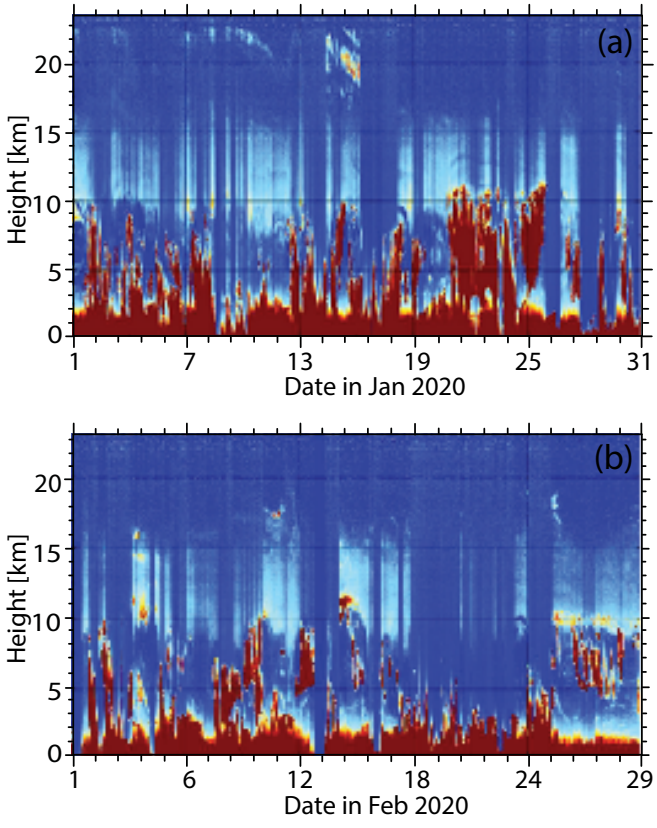

Figure 8. UTLS aerosol layer (light blue layer, 8-16 km) over the North Pole region in (a) January 2020 and (b) February 2020. A few PSCs are visible above 18 km in January and between 15 and 20 km in February. Cirrus (in red) formed in the lower part of the UTLS smoke layer and produced long virga (in red). Below 3 km, Arctic haze prevailed. The range-corrected 532 nm backscatter signal observed with a High Spectral Resolution Lidar aboard Polarstern is shown (HSRL, 2022).

https://doi.org/10.5194/acp-2022-247
Preprint. Discussion started: 12 April 2022

Atmospheric Chemistry and Physics Discussions

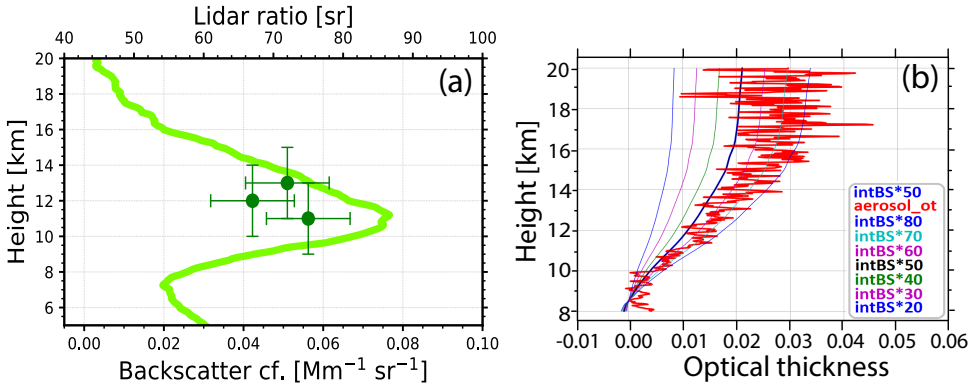

Figure 9. (a) Particle backscatter coefficient (light green, 532 nm, 500 m vertical signal smoothing) and corresponding lidar ratio (dark green circles, 4000 m vertical smoothing, smoothing range is indicated by vertical bars) determined from the Polly observations on 7 February 2020, 00:00-24:00 UTC. Horizontal bars indicate one standard deviation uncertainty. (b) Profile of particle optical thickness (thick red profile) from 8 km up to height z as directly measured with the HSRL at 532 nm (aerosol_ot) and, alternatively calculated from the integral (intBS) of the independently measured backscatter coefficients (above 8 km height up to height z) multiplied by seven different lidar ratios from 20-80 sr. The best match is obtained for a typical wildfire smoke lidar ratio of 70 sr. HSRL signal profiles are averaged for the time period from 7 February 00:00 UTC to 8 February, 05:50 UTC.

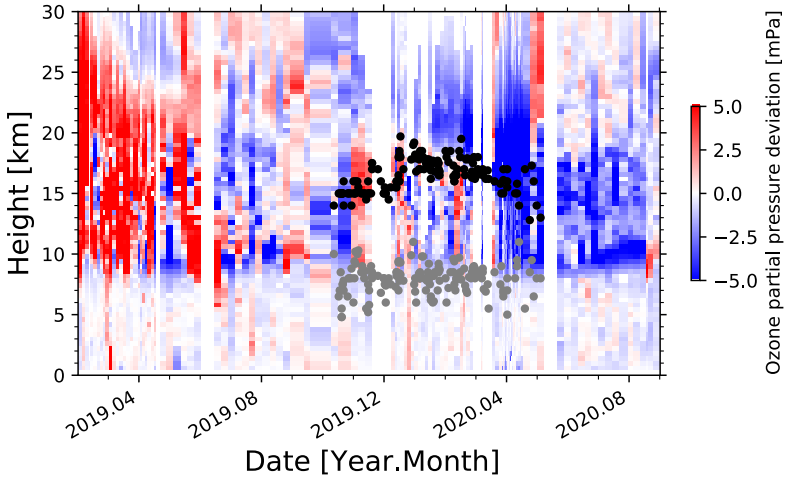

Figure 10. Deviation of each individual ozone profile from the respective long-term (2010-2019) monthly mean ozone profile. Measurements at the Ny-Ålesund (78.9°N) station are used. The base (grey dots) and top heights (black dots) of the Siberian smoke layer measured with Polly aboard Polarstern on a daily basis indicate the smoke-polluted height range.

https://doi.org/10.5194/acp-2022-247
Preprint. Discussion started: 12 April 2022

Atmospheric Chemistry and Physics Discussions

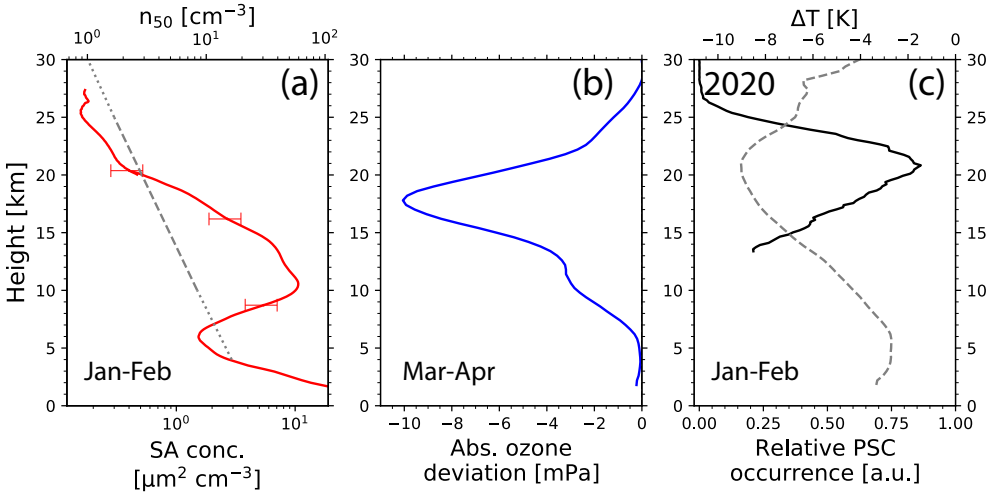

Figure 11. (a) Winter (January-February) mean profiles of the particle surface area (SA) concentration and number concentration n_{50} (particles with radius >50 nm) estimated from lidar observations aboard Polarstern in 2020. Horizontal bars indicate a SA retrieval uncertainty of 35%. Background aerosol estimates are given as a grey dashed-dotted line. (b) Additional ozone loss for March-April 2020, i.e., absolute ozone deviations from the respective long-term March-April (2010-2019) mean ozone profile (see Eq. 2). (c) PSC height range (restricted to heights >13 km) and relative vertical distribution of the PSC frequency of occurrence (in arbitrary units, from CALIOP observations) and mean temperature deviations (dashed line) for the main PSC months January-Februray 2020 from the respective January-February long-term mean profile (calculated with Eq. 5). Ozondesonde data collected at Ny-Ålesund are used in the ozone and temperature calculations.

https://doi.org/10.5194/acp-2022-247
Preprint. Discussion started: 12 April 2022

Atmospheric Chemistry and Physics Discussions

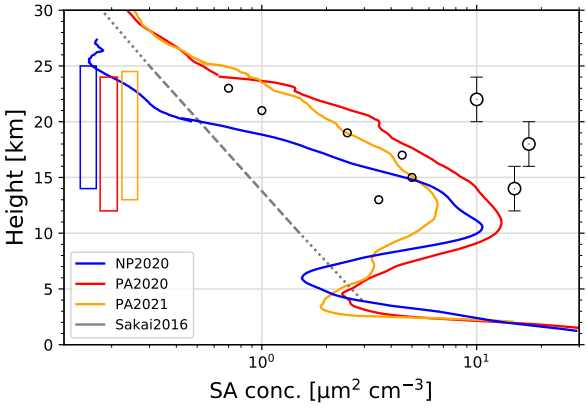

Figure 12. Arctic (NP2020, North Pole, January-February 2020) and Antarctic (PA2020, PA2021, Punta Arenas, June-August 2020, 2021) wildfire smoke layers in terms of particle surface area (SA) concentration. The background aerosol SA concentration is given as well (Sakai et al., 2016). For comparison, SA concentrations observed a few months after the minor Calbuco volcanic eruption (small circles, derived from satellite observations at 55°S, July 2015) (Zhu et al., 2018) and about 1.5 years after the major Pinatubo volcanic eruption (big circles, mean SA concentrations for the height range indicated by vertical bars, 53.4°N, Germany, spring 1993) (Ansmann et al., 1996) are included. PSC occurrence height ranges (open vertical bars to the left) for the Arctic (NP2020, blue) and Antarctic winter seasons (PA2020, red, PA2021, orange) are given as well.

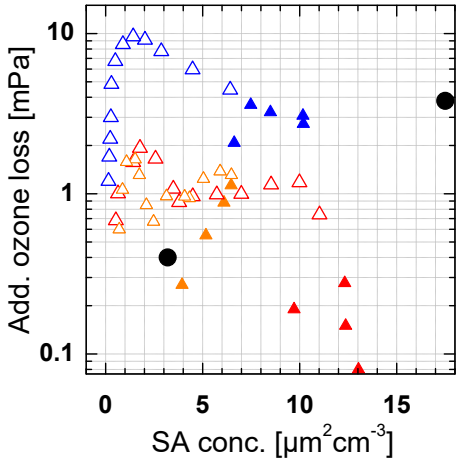

Figure 13. Correlation between smoke particle surface area (SA) concentration and the additional ozone loss observed over the Arctic (blue, 2020) and over Antarctica (red, 2020, orange, 2021). The smoke-ozone data pairs are taken from Figs. 7 and 11. Considered are data from 9-25 km height with a resolution of 1 km (17 data pairs per scenario). Open triangles show PSC-influenced data pairs, closed triangles show the observations below the PSC height range (Arctic, 9-13 km, Antarctica, 9-12 km). For comparison, two values (for PSC free conditions) for volcanic aerosol scenarios are included (Calbuco, low SA conc., Zhu et al. (2018), Pinatubo, high SA conc., Ansmann et al. (1996)).